Tomato geranylgeranyl diphosphate synthase isoform 1 specifically interacts with phytoene synthase isoform 3 to produce strigolactones in tomato roots.

Miguel Ezquerro [1,2], Changseng Li [3], M. Victoria Barja [2], Esteban Burbano-Erazo [1], Julia Pérez-Pérez [1], Yanting Wang [3], Lemeng Dong [3], Purificación Lisón [1], M. Pilar López-Gresa [1], Harro J. Bouwmeester [3], Manuel Rodríguez-Concepción [1,*]

1, Institute for Plant Molecular and Cell Biology (IBMCP), CSIC-Universitat Politècnica de València, 46022 Valencia, Spain

2, Centre for Research in Agricultural Genomics (CRAG) CSIC-IRTA-UAB-UB, Campus UAB Bellaterra, 08193 Barcelona, Spain

3, Plant Hormone Biology group, Green Life Sciences cluster, Swammerdam Institute for Life Sciences, University of Amsterdam, Science Park 904, 1098 XH Amsterdam, the Netherlands

*, Corresponding author: manuelrc@ibmcp.upv.es

Short title: Role of GGPPS isoform 1 in tomato

ORCID numbers: ME, 0000-0002-3051-5502; CL, 0000-0002-9579-4127; MVB, 0000-0002-3846-4885; EB-E, 0000-0001-5056-9893; JP-P, 0000-0001-9448-0700; YW, 0000-0003-1970-4158; LD, 0000-0002-1435-1907; PL, 0000-0002-1662-8084; MPL-G, 0000-0001-9251-0160; HB 0000-0003-0907-2732; MR-C, 0000-0002-1280-2305.

Word count:

1164 Introduction

817 Materials and Methods

4195 Results and Discussion

6176 Total word count for the main body

Datasets:

Number of figures: 9 (all in colour),

Number of tables: 0

Supporting information: 3 Methods, 5 Figures and 3 Tables.

Summary

- Carotenoids are photoprotectant pigments and precursors of the hormones abscisic acid (ABA) and strigolactones (SL). Carotenoids are produced in plastids from geranylgeranyl diphosphate (GGPP), which is diverted to the carotenoid pathway by phytoene synthase (PSY). In tomato (*Solanum lycopersicum*), 3 genes encode plastid-targeted GGPP synthases (*SlG1 to 3*) and 3 genes encode PSY isoforms (*PSY1 to 3*).
- Here we investigated the function of SlG1 by generating loss-of-function lines and combining their metabolic and physiological phenotypes with gene co-expression and co-immunoprecipitation analyses.
- Leaves and fruits of *slg1* lines showed a wild-type phenotype in terms of isoprenoid accumulation, photosynthesis and development. Consistently, *SlG1* is co-expressed with *PSY3* and other genes involved in the production of carotenoids and SL (but not ABA) only in roots. SlG1 was also found to physically interact with the root-specific PSY3 isoform (and not with PSY1 and PSY2). Root SL (but not ABA) levels were reduced in *slg1* lines.
- Our results confirm a specific role of SlG1 in SL production in combination with PSY3. This role appears to be restricted to roots as *slg1* plants do not exhibit the shoot phenotype displayed by other SL-deficient mutants.

Keywords: ABA, carotenoid, GGPP, phytoene synthase, root, strigolactones

Introduction

Isoprenoids are one of the most diverse family of compounds in all living organisms, with plants displaying the highest functional and structural variation (Bouvier et al., 2005). The universal building blocks for the biosynthesis of all isoprenoids are isopentenyl diphosphate (IPP) and its allylic isomer dimethylallyl diphosphate (DMAPP). Both five-carbon (C5) isoprenoid-building molecules are produced in plants by the mevalonic acid (MVA) pathway in the cytosol and the methylerythritol 4-phosphate (MEP) pathway in the plastids (Pulido et al., 2012; Tholl, 2015). Condensation of one or more molecules of IPP to one molecule of DMAPP produces C10 geranyl diphosphate (GPP), C15 farnesyl diphosphate (FPP) and C20 geranylgeranyl diphosphate (GGPP), that are the precursors for most downstream isoprenoid compounds in different cell compartments (Ruiz-Sola & Rodríguez-Concepción, 2012; Zhou & Pichersky, 2020). In the cytosol, FPP is used to synthesize C15 sesquiterpenes and C30 triterpenes required for defensive responses, membrane structure and prenylation of proteins (Thulasiram & Poulter, 2006). In the plastids, GPP is used to make C10 monoterpenes (mostly volatile compounds related to aroma and plant-pathogen interactions) (Chen et al., 2015; Degenhardt et al., 2009) and GGPP is the precursor of gibberellins (GAs) and several photosynthesis-related isoprenoids such as carotenoids, tocopherols, chlorophylls, plastoquinone and phylloquinones (Barja & Rodriguez-Concepcion, 2021). GGPP is also used to produce C20 diterpenes in the cytosol, and both FPP and GGPP are produced in mitochondria from imported MVA-derived IPP and DMAPP for ubiquinone and C20 diterpenoid biosynthesis (Barja & Rodriguez-Concepcion, 2021; Thulasiram & Poulter, 2006).

C40 carotenoids are GGPP-derived plastidial isoprenoids that function as precursors of vitamin A and health-promoting phytonutrients in the human diet and have a great industrial interest as natural pigments (Rodriguez-Concepcion et al., 2018; Ruiz-Sola & Rodríguez-Concepción, 2012). In plants, carotenoids act as photoprotectors in leaves, as pigments in the flowers and fruits of many plant species and as precursors of apocarotenoids, including bioactive compounds such as the hormones abscisic acid (ABA) and strigolactones (SLs) (Al-Babili & Bouwmeester, 2015; Rodriguez-Concepcion et al., 2018). Despite their biological and economic relevance, the factors that integrate and coordinate carotenoid biosynthesis with plant metabolism and development remain little known. In this context understanding how GGPP is channeled to the production of carotenoids for particular functions in diverse tissues, developmental stages and environmental conditions remains a pivotal question.

In plastids, GGPP is produced from MEP-derived IPP and DMAPP by GGPP synthase (GGPPS) enzymes (Figure 1). The first committed and main flux-controlling step of the carotenoid biosynthesis pathway is the condensation of two molecules of GGPP into phytoene catalyzed by phytoene synthase (PSY). Next, phytoene is desaturated and isomerized to lycopene, and the ends of the linear lycopene chain are cyclized to form β-carotene (with two β rings) or α-carotene (with one β and one ε ring). Oxidation of the rings gives rise to xanthophylls such as violaxanthin and neoxanthin from β-carotene or lutein from α-carotene (Figure 1a) (Rodriguez-Concepcion et al., 2018).

In the model plant *Arabidopsis thaliana* PSY is encoded by one gene and the resulting protein directly interacts with AtG11, the main plastidial GGPPS. This interaction likely facilitates the channeling of GGPP to the production of carotenoids (Camagna et al., 2019; Ruiz-Sola et al., 2016a; Ruiz-Sola et al., 2016b). A more complex scenario is found in tomato (*Solanum lycopersicum*). The extra roles associated with carotenoids in this species compared to Arabidopsis (including flower and fruit pigmentation and root mycorrhization) together with genome duplication events have resulted in small PSY and GGPPS gene families. With regard to PSY, tomato has an isoform with a primary role in pigmentation of flowers and ripe fruit (PSY1, Solyc03g031860), another one mainly involved in the production of carotenoids for photosynthesis and photoprotection in leaves (PSY2, Solyc02g081330) and a third one associated to SL and apocarotenoid biosynthesis in roots (PSY3, Solyc01g005940) (Ezquerro et al., 2022; Stauder et al., 2018). From the three plastid-targeted GGPPS isoforms identified in tomato, herein referred to as SlG1 (Solyc11g011240), SlG2 (Solyc04g079960) and SlG3 (Solyc02g085700) (Barja et al., 2021; Zhou & Pichersky, 2020), only SlG2 and SlG3 have been studied in detail. They both produce GGPP for carotenoid synthesis in leaves and fruits, with SlG3 being the main housekeeping isoform and SlG2 acting as a helper enzyme to meet peak demands of GGPP in both organs. SlG2 can be co-immunoprecipitated with both PSY1 and PSY2, but SlG3 cannot (Barja et al. 2021). Although SlG1 is also an active plastid-targeted GGPPS enzyme (Barja et al., 2021; Zhou & Pichersky, 2020), it cannot complement the loss of SlG2 and SlG3 in double mutants, which show an embryo-lethal phenotype like that reported for AtG11-defective Arabidopsis mutants (Ruiz-Sola et al., 2016a; Ruiz-Sola et al., 2016b; Barja et al. 2021). Indeed, *SlG1* transcripts are much less abundant than those of *SlG2* and *SlG3* in most plant tissues (Barja et al., 2021; Zhou & Pichersky, 2020). In leaves, *SlG1* expression is normally low but it is induced following spider mite feeding, wounding and elicitor treatments correlating with the production of defense-related diterpenoid

volatiles (Ament et al., 2006). Other gene expression data suggest that SlG1 might have a role in roots during mycorrhization (Stauder et al., 2018; Barja et al. 2021).

Under nitrogen and/or phosphate starvation, the roots of many plant species (including tomato) exude small quantities of carotenoid-derived SL to promote recognition and colonization by arbuscular mycorrhizal (AM) fungi (Matthys et al., 2016; Stauder et al., 2018; Yoneyama et al., 2008; Zhang et al., 2014). These symbiotic AM fungi help the plant by providing water and mineral nutrients in poor soils, in exchange for carbon products biosynthesized by the plant (Bouwmeester et al., 2007; Yoneyama et al., 2008). Carotenoid metabolism is in turn stimulated in AM roots, resulting in the production of high amounts of pigments such as mycorrhadicins and other apocarotenoids including blumenols, zaxinone and anchorene that modulate the establishment of the AM symbiosis and rhizospheric interactions (Baslam et al., 2013; Fester et al., 2002; Moreno et al., 2021; Stauder et al., 2018). A coordinated role for *SlG1* and *PSY3* has been proposed for SL and AM-associated apocarotenoid biosynthesis in roots, mainly based on expression data (Barja et al., 2021; Stauder et al., 2018). *SlG1* and *PSY3* are indeed the most highly up-regulated genes encoding GGPPS and PSY isoforms when roots are mycorrhized. However, *SlG2* and *PSY1* also show increased transcript levels in mycorrhized roots compared to non-mycorrhized controls (Barja et al., 2021; Stauder et al., 2018). This, together with the observation that the basal expression levels of *SlG1* and *PSY3* in roots is lower than that of *SlG2* and *PSY1* (Barja et al., 2021; Fantini et al. 2013), suggest that more than one isoform of these two enzymes might be providing precursors for carotenoids and derived compounds in roots. To experimentally test this hypothesis and better understand the biological role of SlG1 in tomato, we created CRISPR-Cas9-edited lines defective in SlG1. Here we report their generation and characterization and demonstrate the existence of a highly specific SlG1-PSY3 interaction to produce SL in tomato roots.

Materials and methods

Plant material. Tomato (*Solanum lycopersicum* var. MicroTom) plants were used for experiments. The *ccd7* line, previously referred to as *CCD7-AS*, was made by introgressing a construct expressing a *CCD7* antisense from M82 (Vogel et al., 2010) into MicroTom by successive backcrosses (Pino et al., 2022). Seeds were surface-sterilized by a 30 min water wash followed by a 15 min incubation in 10 ml of 40% bleach with 10 µl of Tween-20. After three consecutive 10 min washes with sterile milli-Q water, seeds were germinated on plates with solid 0.5x Murashige and Skoog (MS)

medium containing 1% agar (without vitamins or sucrose). The medium was supplemented with kanamycin (100 µg/ml) when required to select transgenic plants. Plates were incubated in a climate-controlled growth chamber (Ibercex) at 26°C with a photoperiod of 14 h of white light (photon flux density of 50 µmol m^{-2} s^{-1}) and 10 h of darkness. After 10-14 days, seedlings were transferred to soil and grown under standard greenhouse conditions (14 h light at 25 ± 1 °C and 10 h dark at 22 ± 1 °C). Plants used for root metabolic analysis were grown in a greenhouse with the same conditions but in a mixture of river sand (0.5-1 mm, Filcom BV) and a clay granulate (1:1) instead of soil for easier root collection. For the analysis of phenotypical traits influenced by SLs, fifteen plants were grown for 4 weeks under half strength Hoagland solution and then for 2 additional weeks under half strength Hoagland solution without PO_4^{-3}. *N. benthamiana* plants used for co-immunoprecipitation experiments were grown in the greenhouse under long day conditions at 24°C for 21 days.

Sample collection and phenotypical analyses. Young leaf samples correspond to growing leaflets from the fifth and sixth true leaves and they were collected from soil-grown 4-week-old plants. Chlorophyll fluorescence measurements were carried out with a Handy FluorCam (Photon Systems Instruments). ϕPSII was measure at 30 PAR with an actinic light of 3 µmol m^{-2} s^{-1}. Tomato fruit pericarp samples for isoprenoid quantification were collected at B+3 (three days after breaker). Roots, leaflets and pericarp samples were frozen in liquid nitrogen immediately after collection, freeze-dried and stored at -80 °C. For counting the days from breaker to orange stage, thirty fruits (n=30) from each genotype were chosen and their ripening was monitored *in planta*. For fruit weight determination, 100 ripe fruits from each genotype were collected and weighted one by one using a precision scale (Kern). Fruit volume was estimated in 10 pools of 10 fruits each by measuring the displaced water volume in a graduated cylinder.

Constructs and tomato transformation. For co-immunoprecipitation experiments, full-length cDNAs encoding SlG1 and PSY3 proteins without their stop codons were amplified from root cDNA using the Phusion High-fidelity DNA polymerase (ThermoFisher). Next, the amplicons were introduced via BP clonase into pDONR207 entry plasmid using Gateway (GW) technology (Invitrogen). Full-length sequences were then subcloned through an LR reaction into pGWB414 and pGWB420 plasmids as previously reported (Barja et al., 2021). For CRISPR-Cas9-mediated disruption of

SlG1, two single guide RNAs (sgRNA) (Figure S1-2) were designed using the online tool CRISPR-P 2.0 (Liu et al., 2017). Cloning of the CRISPR-Cas9 constructs was carried out as previously described (Barja et al., 2021) using primers listed in Table S1. As a result, a single final binary plasmid harboring the Cas9 sequence, the NPTII gene providing kanamycin resistance, and the sgRNAs was obtained and named pDE-Cas9-SlG1 (Table S2). All constructs were confirmed by restriction mapping and DNA sequencing. *Agrobacterium tumefaciens* GV3101 strain was used to stably transform tomato MicroTom cotyledons with pDE-Cas9-SlG1 as described (Ezquerro et al., 2022). *In vitro* regenerated T1 lines were identified based on kanamycin resistance (100 µg/ml) PCR genotyping and sequencing (Table S1). Homozygous T2 lines lacking Cas9 were obtained after segregation and stable T3 offspring was used for next experiments.

Metabolite and gene expression analyses. Plastidial isoprenoids (carotenoids, chlorophylls, tocopherols), hormones (ABA, SL) and volatile organic compounds was carried out as described (Methods S1). Gene co-expression network**s** and RT-qPCR analyses were performed as described (Methods S2).

***P. syringae* infection of tomato plants.** *Pseudomonas syringae pv. tomato DC3000* (*Pst*) strain were used for tomato infection as previously reported (López-Gresa et al., 2018). Briefly, bacteria were grown during 48 h at 28°C in LB agar medium with rifampicin (10 mg/mL) and kanamicin (0.5 mg/mL). When colonies appeared, they were transferred to King's B liquid medium supplemented with antibiotics and grown overnight at 28°C. Next, bacteria were centrifugated at 3000 x*g* for 15 min and resuspended in 10mM $MgCl_2$ at a final optical density of 0.1 for further infection. Inoculation with bacteria was carried out in 4-week-old MicroTom plants without flowers by immersion. Plants were dipped into the bacterial suspension containing 0.05% Silwet L-77 for 30 seconds and left 24 hours for subsequent sample collection.

Co-immunoprecipitation assays. Co-immunoprecipitation experiments were carried out as described (Barja & Rodríguez-Concepción, 2020; Barja et al., 2021) (Methods S3).

Results and discussion

Generation of CRISPR lines defective in SlG1

The approach followed to create *SlG1*-defective mutants by CRISPR-Cas9 was very similar to the one followed to generate *slg2* and *slg3* mutants (Barja et al., 2021). Briefly, we designed two single guide RNAs (sgRNA) (see Table S1 and S2 for primer and construct details) with CRISPR-P 2.0 (Liu et al., 2017) to create a small deletion that would disrupt the intronless *SlG1* gene (Figure 1). After transformation of tomato MicroTom plants and genotyping, two independent mutant alleles without Cas9 were selected and named *slg1-1* and *slg1-2* (Figure 1b).

The *slg1-1* allele has a deletion that causes a frameshift and a premature translation stop codon (Figure 1b and Figures S1-S2). The resulting protein lacks the C-terminal region containing the second Asp-rich motif (SARM, essential for prenyl-transferase function) and it is smaller than the wild-type (WT) enzyme (226 aa instead of 365 aa). A longer deletion in the *slg1-2* allele maintains the open reading frame and produces a 253 aa chimeric protein that lacks a fragment of the WT enzyme containing the SARM (Figure 1b and Figures S1-S2). Similar mutations lacking the C-terminal part of the protein and the SARM were previously shown to result in complete loss of GGPPS activity in *slg2* mutants (Barja et al., 2021). Therefore, we considered these two alleles as knock-out mutants and selected them for the rest of experiments.

Loss of SlG1 does not impair the production of photosynthesis-related isoprenoids in tomato leaves.

SlG1 is expressed at low levels in all tomato plant tissues, including leaves (Figure S3). To investigate possible roles of SlG1 in leaves, we first analyzed the levels of GGPP-derived plastidial isoprenoids in *slg1* lines under normal growth conditions (Figure 2). Lines lacking SlG2 (*slg2-1*) or SlG3 (*slg3-1*) were grown together with the SlG1-defective mutants and WT controls for comparison. Young and mature leaves of *slg1-1* and *slg1-2* plants appeared very similar to those from *slg2* and WT plants (Figure 2a). By contrast, young emerging leaves from *slg3* plants showed a paler green color as previously reported (Barja et al., 2021). The color phenotype of young leaves correlated with their photosynthetic pigment (carotenoids and chlorophylls) content (Figure 2b) and their photosynthetic activity estimated as effective quantum yield of photosystem II (ϕPSII) (Figure 2c), which were only reduced in the *slg3* mutant. Tocopherol levels, by contrast, were similar in all the lines, although a trend towards lower levels was detected in young leaves of the *slg3* mutant, as previously reported

(Barja et al., 2021). The described results are in agreement with our previous conclusion that *SlG3* is the main isoform in suppling GGPP for photosynthesis-related isoprenoids in leaves under normal growth conditions (Barja et al., 2021). A role for SlG2 in providing extra GGPP to support the production of these isoprenoids when needed, e.g., during deetiolation, was proposed in part based on gene expression data (Barja et al., 2021). Unlike *SlG2*, however, *SlG1* is poorly co-expressed with isoprenoid biosynthetic genes in leaves and it is not induced during seedling deetiolation (Barja et al., 2021), supporting the conclusion that SlG1 does not substantially contribute to GGPP production in chloroplasts.

SlG1 is not required for monoterpene synthesis in leaves.

Leaves are mainly photosynthetic organs but they also contain cell types lacking chloroplasts. In particular, tomato leaves contain large amounts of glandular trichomes formed by non-photosynthetic cells that produce large amounts of volatile organic compounds (VOCs), including many of isoprenoid origin (Schuurink and Tissier, 2020). *SlG1* but also *SlG2* and *SlG3* are expressed in leaf trichomes (Zhou & Pichersky, 2020). The main groups of isoprenoid VOCs are MVA-derived sesquiterpenes (made from C15 FPP), MEP derived monoterpenes (made from C10 GPP or nerolidol diphosphate, NPP) and diterpenes (made from C20 GGPP). A role for SlG1 in the production of GGPP-derived diterpene VOCs was investigated following the observation that *SlG1* expression was induced by treatments that stimulated the production of such VOCs (Ament et al., 2006). Our data mining of the database Genevestigator found that *SlG1* expression is also upregulated in leaves after infection with the bacterium *Pseudomonas syringae pv. tomato* DC3000 (*Pst*), whereas *SlG2* and *SlG3* transcript levels remained unchanged (Figure S4). The most prominent isoprenoid VOCs produced upon *Pst* infection are monoterpenes such as linalool, limonene and α-terpineol (Lopez-Gresa et al., 2017; Zhou & Pichersky, 2020). Linalool is produced from GPP synthesized by homodimeric GPP synthases such as tomato GPPS (Solyc08g023470) or heterodimeric enzymes formed by a GGPPS subunit and the small subunit type I (SSU-I) protein (Solyc07g064660), whereas limonene and α-terpineol derive from NPP produced by the NPP synthase NDPS1/CPT1 (Solyc08g005680) (Schilmiller et al., 2009) (Figure 3a). Similar to *SlG1*, tomato *NDPS1*, *GPPS* and *SSU-I* genes are induced in *Pst*-infected leaves, with *SlG1, SSU-I* and *NDPS1* showing the strongest upregulation (Figure S4). SlG1/SSU-I heterodimers have been shown to mainly produce GPP *in vitro* (Zhou & Pichersky, 2020) and SlG2/SSU-I heterodimers have been found to produce GPP for monoterpene

biosynthesis in tomato fruit (Hivert et al., 2020). Based on these data, we hypothesized that SlG1 might participate in the production of monoterpenes in leaves.

To test this hypothesis, we infected WT and GGPPS-defective tomato plants with *Pst* and quantified the levels of several monoterpenes (and a sesquiterpene as a control) before and 24 h after the infection (Figure 3b). Strikingly, bacterial infection did not cause significant changes in monoterpene or sesquiterpene levels in WT plants or any of the mutants tested (Figure 3b) even though a clear upregulation of *SlG1* expression was observed (Figure 3c). Surprisingly, *SlG2* transcript levels decreased in *Pst*-infected WT samples (Figure 3c) while *slg2* mutants contained increased basal levels of all VOCs analyzed (Figure 3b). These results suggest that impairment of SlG2 activity results in higher production and/or accumulation of these VOCs, which are derived from IPP and DMAPP from different origins: the MVA pathway (via FPP) and the MEP pathway (via NPP or GPP). However, the levels of leaf isoprenoid products made from MEP-derived GGPP (carotenoids, chlorophylls, tocopherols) were similar in *slg2* and WT lines (Figure 2b) (Barja et al., 2021). We speculate that loss of SlG2 function in trichomes (the VOC-producing cells in the leaf) might cause the diversion of SlG2 substrates (i.e., IPP and DMAPP) to the production of VOCs. Alternatively, a metabolic imbalance or a defense response in *slg2* plants that cannot be rescued by SlG1 or SlG3 might eventually lead to VOC overproduction.

Unlike the results from Genevestigator RNA-seq data (Figure S4), in our experiment we did not detect any changes in the levels of *SSU-I* transcripts (Figure 3c). This Genevestigator differential expression profile might be a consequence of different genetic backgrounds used in the experiments. In agreement with this hypothesis, *SSU-I* transcript levels are very low in cultivated tomatoes (*S. lycopersicum*) but are abundant in the fruits of wild relatives (*S. pimpinellifolium* and *S. cheesmaniae*), which produce substantially more monoterpenes (Hivert et al., 2020). Whereas MicroTom has been broadly used for infection experiments with some bacteria and fungi (Costa et al., 2021; Deganello et al., 2014; Nakahara et al., 2016), previous experiments using *Pst* found no wilt symptoms or bacterial growth eight days after infection (Takahashi et al., 2005), strongly suggesting that *Pst* is just an opportunistic MicroTom pathogen. This suggests that tomato MicroTom is not the best genotype to investigate the molecular and metabolic changes triggered by *Pst* infection. However, the similar levels of monoterpenes found in non-infected leaves of WT and SlG1-defective alleles argues against a role of SlG1 in the production of these plastidial isoprenoids in leaves.

SlG1 is dispensable for carotenoid biosynthesis in fruit.

Carotenoids are synthesized at very high rates during tomato fruit ripening, contributing together with the degradation of chlorophylls to progressively change the fruit color from green at the mature green (MG) stage to orange (O) and eventually red at the ripe (R) stage. The first visual symptoms of color change define the breaker (B) stage. *SlG1* is expressed at very low levels during fruit ripening (Figure S3), when GGPP produced by SlG3 and upregulated levels of *SlG2* support carotenoid overproduction (Barja et al., 2021). Reduced activity of SlG2 and SlG3 results in lower levels of lycopene (the main carotenoid accumulated during ripening) in R fruit collected at 10 days after the B stage (B+10) but only SlG3-defective lines showed significantly decreased levels of total carotenoids at this stage and none of the mutants showed differences with the WT in MG fruit (Barja et al., 2021). When we measured carotenoid levels in B+3 fruits (*i.e.,* between O and R stages), WT levels of total carotenoids were found in *slg1* and *slg2* lines, whereas *slg3* fruits showed significantly lower levels (Figure 4a). In particular, phytoene and lycopene contents were strongly reduced in *slg3* fruits, whereas β-carotene levels were similar to those of WT controls (Figure 4a). The absence of significant differences in carotenoid levels among WT, *slg1* and *slg2* fruit at the B+3 stage (Figure 4a) suggests that SlG3 is the main GGPP provider in the early stages of fruit ripening. As ripening advances, up-regulation of SlG2 contributes with extra GGPP. The WT phenotype of SlG1-deficient mutant fruits together with the lack of gene expression changes during ripening support the conclusion that this isoform does not contribute to GGPP for carotenoid production in fruit.

Lower levels of the carotenoid-derived hormone ABA were measured in the fruit pericarp of tomato mutants lacking SlG2 and particularly SlG3, eventually contributing to a delay in ripening (Barja et al., 2021). Consistently, the number of days that B fruits needed to reach the O stage was higher in *slg2* and *slg3* lines compared to WT controls (Figure 4b). ABA has also been shown to promote fruit growth (McQuinn et al., 2020; Zhang et al., 2009; Ezquerro et al. 2022). Reduced ABA contents in *slg2* and *slg3* fruit pericarp (Barja et al., 2021) actually correlate with a reduced fruit volume of ripe fruit, although this was only statistically significant for *slg3* fruits and it did not affect fruit weight (Figure 4c). Again, *slg1* fruits were undistinguishable from WT controls (Figure 4c). The observation that losing SlG1 activity does not impact any of the fruit phenotypes tested strongly supports the conclusion that this isoform is dispensable for the production of GGPP for carotenoids and related metabolites during fruit ripening.

Gene co-expression analysis suggests a major role for SlG1 in roots.

In our previous work we demonstrated that *SlG2* and, to a lower extent, *SlG3* expression were highly connected to the expression of plastidial isoprenoid biosynthetic genes in leaf tissue. In fruits, *SlG3* had a higher connection than *SlG2* to genes from these metabolic pathways (Barja et al., 2021). The correlation of *SlG1* with other plastidial isoprenoid genes was very poor in leaves as well as in fruits. Other gene expression data suggested that *SlG1* might function in roots to produce SL or/and AM-related apocarotenoids (Stauder et al., 2018; Barja et al. 2021). To provide further evidence for this hypothesis, we performed a gene co-expression network (GCN) analysis in roots. We used publicly available data for plant comparative genomics (PLAZA 4.0 Phytozome) to look for tomato homologues of genes for plastidial isoprenoid biosynthesis and related pathways. We obtained the expression data of such tomato homologs from recently published tomato RNA-seq data in root tissue (Wang et al., 2021) and calculated their expression correlation with *SlG1*, *SlG2* and *SlG3* expression using pairwise Pearson correlations as previously reported (Wang et al., 2022). Results are shown in Figure 5 and correlations and gene details are listed in Table S3. Opposite to that observed in leaf tissue, *SlG2* displays a low correlation with other isoprenoid biosynthetic genes in roots (Figure 5). *SlG3* shows a medium connectivity to many of the selected genes, probably because it is the isoform providing GGPP for housekeeping functions (Barja et al., 2021). Intriguingly, *SlG1* showed high correlation with many genes of the MEP and the carotenoid pathways as well as with most of the genes involved in SL biosynthesis, while it showed limited connectivity with genes converting carotenoids into ABA (Figure 5). These results suggest that gene expression is coordinated such that SlG1-derived root carotenoids are channeled into the production of SLs but not ABA. *SlG1* connectivity was also very high with GA biosynthetic genes. GAs are GGPP-derived phytohormones that appear to act together with SLs during the P-starvation response (Wang et al., 2021) and root mycorrhization (Nouri et al., 2021; Ruiz-Lozano et al., 2016), promoting root growth to help establishment of AM symbiosis. A tight correlation between SLs and the expression of GA-related genes has been reported (Wang et al., 2021), suggesting that the observed co-expression of *SlG1* with GA biosynthetic genes might be a secondary effect.

SlG1 specifically interacts with PSY3

Gene expression data and our GCN analysis (Figure 5), support the conclusion that SlG1 might function in coordination with PSY3 to produce SL and likely other AM-

associated apocarotenoids (but not ABA) in roots (Barja et al., 2021; Stauder et al., 2018). GGPPS proteins have been shown to physically interact with PSY enzymes in different plant species (Ruiz-Sola et al., 2016b; Wang et al., 2018; Camagna et al., 2019; Barja et al., 2021). In tomato, co-immunoprecipitation experiments in *Nicotiana benthamiana* leaves showed direct interaction of SlG2 with PSY1 and PSY2, while no interaction with these PSY isoforms was found for SlG3 even though the latter was shown to homodimerize and heterodimerize with SlG2 using the same experimental design (Barja et al., 2021). To extend the tomato GGPPS-PSY interaction map with SlG1, we performed co-immunoprecipitation assays *in planta* using Myc-tagged GGPPS and HA-tagged PSY proteins (Figure 6). Tagged proteins were transiently expressed in *N. benthamiana* leaves by agroinfiltration and then protein extracts were used to confirm the presence of the recombinant enzymes (Figure 6a) and for co-immunoprecipitation with anti-Myc antibodies followed by immunoblot analysis with both anti-Myc and anti-HA antibodies (Figure 6b). A Myc-tagged phosphoribulokinase protein from Arabidopsis (PRK-Myc) was used as a negative control (Barja et al., 2021). Additionally, a SlG1-HA construct used together with SlG1-Myc confirmed that SlG1 forms homodimers and that the Myc-tagged version allowed to co-immunoprecipitate protein partners (Figure S5). When combined with PSY isoforms, SlG1 was found to only co-immunoprecipitate with PSY3, whereas SlG2 and SlG3 were unable to interact with this particular isoform (Figure 6b).

It has been suggested that PSY enzymes cannot access freely diffusible plastidial GGPP because of their specific plastid location attached to membranes (Camagna et al., 2019), making interaction among GGPPS and PSY enzymes necessary for GGPP channeling into the carotenoid pathway. Strikingly, the tomato housekeeping isoform SlG3 is unable to directly interact with any of the PSY isoforms present in tomato (Figure 6b) (Barja et al., 2021). However, there are several possibilities for an indirect interaction of SlG3 with PSY enzymes (Barja & Rodriguez-Concepcion, 2021). Heterodimerization of SlG2 and SlG3 might allow interaction of SlG3 with PSY1 or PSY2 via SlG2 (Barja et al., 2021), whereas possible heterodimerization of SlG1 and SlG3 might allow interaction with PSY3 (Figure 6b). Another mechanisms that could potentially facilitate the GGPP - PSY interaction could be interaction with the small subunit type II (SSU-II) protein (Solyc09g008920), a catalytically inactive polypeptide shown to interact with different GGPPS enzymes to improve their GGPP production (Wang et al., 2018; Zhou et al., 2017; Zhou & Pichersky, 2020) but also to stimulate the interaction with PSYs (Wang et al., 2018). While the described interactions potentially allow any of the three tomato GGPPS isoforms to form a complex with any of the PSY

isoforms, it is expected that direct interactions (SlG1-PSY3, SlG2-PSY1 and SlG2-PSY2) would be most efficient to convert GGPP into phytoene. In the case of SlG1 and PSY3, this interaction is strengthened by the coordinated expression profiles of the corresponding genes in roots upon phosphate starvation and mycorrhization with AM fungi (Figure 5) (Barja et al., 2021; Stauder et al., 2018) and this strongly supports the conclusion that these isoforms share the same functional role(s).

SL synthesis is impaired in *slg1* and *psy1* mutants

To experimentally confirm the role of the different GGPPS and PSY isoforms in the production of carotenoid precursors for SL or/and ABA biosynthesis in roots, we analyzed the levels of these metabolites in WT plants and mutant lines defective in GGPPS and PSY isoforms. In the latter case, only CRISPR-Cas9 lines lacking PSY1 (*psy1-2*) and PSY2 (*psy2-1*) were used (Ezquerro et al., 2022), as PSY3-defective lines are not available. As a control, we used a tomato MicroTom line with a silenced *CCD7* gene (Solyc01g090660), encoding the SL biosynthetic enzyme carotenoid-cleavage dioxygenase 7 (Pino et al., 2022). This line, herein named *ccd7*, shows a highly branched phenotype consistent with expectedly low SL production (Pino et al., 2022). We grew the plants in half-strength Hoagland solution either containing normal phosphate (+P) or without phosphate (-P) to induce SL synthesis and measured carotenoid and ABA levels in root tissues and SL levels in root exudates (Figure 7). Carotenoid levels measured in roots were very low in all genotypes both under +P and -P conditions (Figure 7a). Only the *ccd7* line displayed statistically significant changes between conditions, as carotenoid levels increased under phosphate starvation (Figure 7a).

Next, we measured the levels of the carotenoid-derived phytohormone ABA in the same samples used for carotenoid quantification. Consistent with our GCN data showing no correlation of ABA biosynthetic genes with any of the tomato genes for GGPPS isoforms (Figure 5), none of the GGPPS-defective mutants presented statistically significant differences in root ABA levels in either +P or -P conditions compared to WT controls (Figure 7b). Interestingly, ABA levels were higher in roots of *psy1-2* and *psy2-1* plants grown under +P and –P conditions (Figure 7b). Analysis of gene expression levels by qRT-PCR showed that loss of PSY1 and PSY2 activities did not substantially increase the expression of any remaining PSY-encoding gene or any GGPPS-encoding gene in roots (Figure 8). We therefore conclude that other genes involved in ABA synthesis might be upregulated in *psy1* and *psy2* roots. Alternatively,

loss of PSY1 or PSY2 in roots might cause a metabolic imbalance that cannot be rescued by the remaining PSY isoforms and eventually leads to ABA overproduction.

The levels of several SLs were next measured in root exudates from plants grown under phosphate starvation for seven days (Figure 7c). All SL measured (except for oxo-orobanchol which also displays a trend towards lower levels) were significantly reduced in both *slg1* mutant alleles compared to WT controls, confirming a major role for the SlG1 isoform in producing GGPP precursors for these carotenoid-derived hormones. Exudates from *slg2-1* and *slg3-1* roots contained WT levels of SLs (Figure 7c). However, the observation that none of the two null *slg1* mutant alleles showed a complete absence of SLs suggest that SlG2 or/and SlG3 can also contribute to SL production, at least when SlG1 activity is absent. Because a role for PSY3 in root SL production has been demonstrated in the legume *Medicago truncatula* and suggested in tomato (Stauder et al., 2018), we expected WT levels of SLs in mutants defective in PSY1 and PSY2, which harbor a functional PSY3 enzyme. However, *psy1-2* displayed a very similar reduction in SL levels to that detected in *slg1*, suggesting that PSY1 may also have a role in SL synthesis in tomato roots (Figure 7c). In agreement, *PSY1* basal expression levels in roots are higher than those of *PSY3* (Barja et al., 2021; Fantini et al. 2013) and they increase in mycorrhized roots compared to non-mycorrhized controls (Barja et al., 2021; Stauder et al., 2018). Strikingly, in PSY1-defective roots SlG1 expression was not upregulated under phosphate starvation (Figure 8), suggesting that this might be the main cause of the low SL levels produced by the *psy1-2* mutant (Figure 7c). This result also reinforces the conclusion that SlG1 has a central role in SL production in roots. Furthermore, upregulation of *PSY3* expression under phosphate starvation was also reduced (but not impaired) in *psy1-2* roots, similar to that observed in SlG1-defective roots (Figure 8). This result suggests that SLs might feedback promote *PSY3* expression. Alternatively, the absence of SlG1 (in *slg1* mutants) or the failure to upregulate its levels under phosphate starvation (in *psy1* mutants) might be the reason why *PSY3* expression also becomes less responsive to phosphate starvation. As SlG1 and PSY3 isoforms physically interact (Figure 6), it is not surprising that their transcription is coordinated. In any case, the data strongly support a central role for SlG1 and PSY3 in root SL production.

SL reduction in *slg1* and *psy1* roots does not affect aerial plant architecture

SLs are plant phytohormones that regulate developmental processes in roots, shoot and leaves. They promote root hair elongation, lateral root outgrowth and primary root

growth and inhibit adventitious root formation (Al-Babili & Bouwmeester, 2015; Matthys et al., 2016; Ruyter-Spira et al., 2011; Kohlen et al., 2012). In shoots, they promote secondary growth and inhibit auxiliary bud branching (Gomez-Roldan et al., 2008; Ruyter-Spira et al., 2013), and in leaves they promote leaf senescence together with other plant hormones (Ueda & Kusaba, 2015; Yamada & Umehara, 2015). While increased branching is one of the most conspicuous phenotypes caused by reduced SL levels, a visual inspection could not detect any obvious branching phenotype in greenhouse-grown plants of any of our CRISPR-Cas9-edited lines.

To obtain quantitative data, we measured several phenotypic parameters related with SL-regulated plant growth in these lines grown together with WT controls and SL-deficient *ccd7* plants (Pino et al., 2022; Vogel et al., 2010). Measurements were performed on fifteen plants per genotype grown under +P for four weeks and then transferred to -P for two more weeks to promote SL biosynthesis (Ruyter-Spira et al., 2013) (Figure 9). Dry root weight was reduced in SL-deficient *slg1-1*, *slg1-2*, *psy1-2* and *cdd7* lines compared to WT controls and mutants with normal SL production, i.e., *slg2-1*, *slg3-1* and *psy2-1* plants (Figure 9a). These data confirm that SLs have a role in promoting root growth (Al-Babili & Bouwmeester, 2015; Ruyter-Spira et al., 2013). Next, we measured the height of the plants and observed that *ccd7* plants were smaller than WT plants (Figure 9b). Surprisingly, the SL-deficient mutants (*slg1-1*, *slg1-2* and *psy1-2*) showed a very similar size as WT plants, whereas *slg2-1* and *slg3-1*, which produced normal levels of SLs in roots, were smaller (Figure 9b). The reduced size of *slg2-1* and *slg3-1* plants might be derived from their metabolic imbalances resulting from suboptimal photosynthesis (Barja et al., 2021). SL-synthesis mutants typically are dwarfs with increased numbers of lateral branches (Gomez-Roldan et al., 2008; Yamada et al., 2014). Indeed, *ccd7* plants not only were smaller (Figure 9b) but also displayed a higher number of lateral branches compared to WT controls in our experimental conditions (Figure 9c), consistent with previous reports by other groups (Pino et al., 2022; Vogel et al., 2010). In agreement with our preliminar visual observations, none of the mutants defective in GGPPS or PSY isoforms showed a branching phenotype (Figure 9c). The results indicate that only *ccd7* plants display a SL deficiency shoot phenotype, probably because constitutive silencing of the *CCD7* gene affects SL production in all plant tissues. By contrast, loss of SlG1 appears to only affect SL production in roots, impacting root growth but not shoot growth or branching. The similar phenotypes of *slg1-1*, *slg1-2* and *psy1-2* plants further support the conclusion that the reduced SL production by PSY1-defective roots is due to a block in *SlG1* upregulation rather than caused by decreased PSY1 activity. It is

commonly accepted that SLs are synthetized in plant roots and from there transported to aerial parts, where they regulate plant growth and shoot branching (Al-Babili & Bouwmeester, 2015; Gomez-Roldan et al., 2008; Ruyter-Spira et al., 2013). Nevertheless, grafting studies in tomato and pea have shown that the SL biosynthetic machinery is active in stems and can produce SLs that are transported via the xylem to shoots and leaves (Beveridge et al., 2009; Visentin et al., 2016; Xie et al., 2010). As the expression levels of *SlG1* in aerial parts under normal conditions are very low (about 40-fold lower than *SlG2* and 50-fold lower than *SlG3*) (Figure S3) (Barja et al., 2021; Stauder et al., 2018), we propose that SlG1 is exclusively involved in providing GGPP for SL synthesis in roots. In shoots, much higher levels of carotenoids (derived from GGPP made by SlG2 and/or SlG3) may supply enough precursors to produce SLs supporting normal aboveground growth and development.

Concluding remarks

In summary, extensive characterization of tomato lines defective in the SlG1 isoform only found a clear phenotype in the root, consistent with the high connectivity of *SlG1* to other isoprenoid-related genes in roots but not in shoot tissues. Specifically, SlG1 appears to act together with PSY3 exclusively in the roots to eventually produce SLs but not other carotenoid-derived hormones such as ABA. SLs released by plant roots to the soil are well-known signaling molecules for colonization by AM fungi but also for germination of parasitic plants (Bouwmeester et al., 2021; López-Ráez et al., 2009; Yoneyama et al., 2008). The particular characteristics of the *slg1* mutant make it an attractive target for breeding to negate the negative effects associated to infection by parasitic plants without altering normal shoot growth and metabolism, including photosynthesis and fruit ripening.

Acknowledgments

We thank Mª Rosa Rodriguez-Goberna for technical help with HPLC analyses, Kristýna Floková for the support with ABA measurements, Ernesto Llamas for providing the pGWB417_AtPRK construct, Rodrigo Therezan and Lazaro E.P. Peres (USP, Brazil) for the tomato *ccd7* line, and Albert Ferrer and Laura Gutiérrez for the pDE-Cas9 (with kanamycin resistance) plasmid. This work was funded by grants from Spanish MCIN/AEI/10.13039/501100011033 and European NextGeneration EU/PRTR and PRIMA programs to MR-C (PID2020-115810GB-I00 and UToPIQ-PCI2021-121941). MR-C is also supported by CSIC (202040E299) and Generalitat Valenciana (PROMETEU/2021/056). ME received a predoctoral fellowship from MCIN/AEI (BES-2017-080652) and an EMBO Scientific Exchange Grant (9315). No conflict of interest is declared.

Author Contributions

ME and MR-C designed the research; ME, CL, MVB, EB-E, JP-P and YW performed research; LD, MPL-P, PL and HB contributed new analytic tools; ME, CL, MVB, EB-E, JP-P, YW, LD, PL, MPL-G, HB and MR-C analyzed and discussed data; ME and MR-C wrote the paper and incorporated the input of the rest of the authors.

Competing interests

None declared.

Data availability

The data that supports the findings of this study are available in the supplementary material of this article.

References

Al-Babili, S., & Bouwmeester, H. J. (2015). Strigolactones, a novel carotenoid-derived plant hormone. *Annual Review of Plant Biology*, *66*, 161–186.

Ament, K., van Schie, C. C., Bouwmeester, H. J., Haring, M. A., & Schuurink, R. C. (2006). Induction of a leaf specific geranylgeranyl pyrophosphate synthase and emission of (E,E)-4,8,12-trimethyltrideca-1,3,7,11-tetraene in tomato are dependent on both jasmonic acid and salicylic acid signaling pathways. *Planta*, *224*(5), 1197–1208.

Barja, M. V., Ezquerro, M., Beretta, S., Diretto, G., Florez-Sarasa, I., Feixes, E., Fiore, A., Karlova, R., Fernie, A. R., Beekwilder, J., & Rodríguez-Concepción, M. (2021). Several geranylgeranyl diphosphate synthase isoforms supply metabolic substrates for carotenoid biosynthesis in tomato. *New Phytologist*, *231*(1), 255–272.

Barja, M. V., & Rodriguez-Concepcion, M. (2021). Plant geranylgeranyl diphosphate synthases: every (gene) family has a story. *aBIOTECH, Springer*, 2(3), 289-298.

Baslam, M., Esteban, R., García-Plazaola, J. I., & Goicoechea, N. (2013). Effectiveness of arbuscular mycorrhizal fungi (AMF) for inducing the accumulation of major carotenoids, chlorophylls and tocopherol in green and red leaf lettuces. *Applied Microbiology and Biotechnology*, 97(7), 3119–3128.

Beveridge, C. A., Dun, E. A., & Rameau, C. (2009). Pea has its tendrils in branching discoveries spanning a century from auxin to strigolactones. *Plant Physiology*, *151*(3), 985–990.

Bouvier, F., Rahier, A., & Camara, B. (2005). Biogenesis, molecular regulation and function of plant isoprenoids. *Progress in Lipid Research,* 4(6), 357-429.

Bouwmeester, H., Li, C., Thiombiano, B., Rahimi, M., & Dong, L. (2021). Adaptation of the parasitic plant lifecycle: Germination is controlled by essential host signaling molecules. *Plant Physiology* 185(4),1292-1308

Bouwmeester, H. J., Roux, C., Lopez-Raez, J. A., & Bécard, G. (2007). Rhizosphere communication of plants, parasitic plants and AM fungi. *Trends in Plant Science*, 12(5), 224–230.

Camagna, M., Grundmann, A., Bar, C., Koschmieder, J., Beyer, P., & Welsch, R. (2019). Enzyme fusion removes competition for geranylgeranyl diphosphate in carotenogenesis. *Plant Physiology*, 179(3), 1013–1027.

Chen, Q., Fan, D., & Wang, G. (2015). Heteromeric geranyl(geranyl) diphosphate synthase is involved in monoterpene biosynthesis in arabidopsis flowers. *Molecular Plant*, 8(9), 1434–1437.

Costa, J. L., Paschoal, D., da Silva, E. M., Silva, J. S., do Carmo, R. M., Carrera, E., López-Díaz, I., Rossi, M. L., Freschi, L., Mieczkowski, P., Peres, L. E. P., Teixeira, P. J. P. L., & Figueira, A. (2021). *Moniliophthora perniciosa*, the causal agent of witches' broom disease of cacao, interferes with cytokinin metabolism during infection of Micro-Tom tomato and promotes symptom development. *New Phytologist*, 231(1), 365–381.

Deganello, J., Leal, G. A., Rossi, M. L., Peres, L. E. P., & Figueira, A. (2014). Interaction of moniliophthora perniciosa biotypes with micro-tom tomato: A model system to investigate the witches' broom disease of theobroma cacao. *Plant Pathology*, *63*(6), 1251–1263.

Degenhardt, J., Köllner, T. G., & Gershenzon, J. (2009). Monoterpene and sesquiterpene synthases and the origin of terpene skeletal diversity in plants. *Phytochemistry*, 70 (15), 1621–1637.

Ezquerro, M., Burbano, E., & Rodríguez-Concepción, M. (2022) Overlapping and specialized roles of tomato phytoene synthase isoforms PSY1 and PSY2 in carotenoid and ABA production. *bioRxiv* doi: 10.1101/2022.08.11.503628.

Fantini, E., Falcone, G., Frusciante, S., Giliberto, L., & Giuliano, G. (2013). Dissection of tomato lycopene biosynthesis through virus-induced gene silencing. *Plant Physiology*, 163(2), 986–998.

Fester, T., Schmidt, D., Lohse, S., Walter, M. H., Giuliano, G., Bramley, P. M., Fraser, P. D., Hause, B., & Strack, D. (2002). Stimulation of carotenoid metabolism in arbuscular mycorrhizal roots. *Planta,* 216(1), 148–154.

Floková, K., Tarkowská, D., Miersch, O., Strnad, M., Wasternack, C., & Novák, O. (2014). UHPLC–MS/MS based target profiling of stress-induced phytohormones. *Phytochemistry*, 105, 147-157.

Gomez-Roldan, V., Fermas, S., Brewer, P. B., Puech-Pagès, V., Dun, E. A., Pillot, J. P., Letisse, F., Matusova, R., Danoun, S., Portais, J. C., Bouwmeester, H., Bécard, G., Beveridge, C. A., Rameau, C., & Rochange, S. F. (2008). Strigolactone inhibition of shoot branching. *Nature*, 455(7210), 189–194.

Hivert, G., Davidovich-Rikanati, R., Bar, E., Sitrit, Y., Schaffer, A., Dudareva, N., & Lewinsohn, E. (2020). Prenyltransferases catalyzing geranyldiphosphate formation in tomato fruit. *Plant Science*, 296, 110504

Kohlen, W., López Ráez, J.A., Pollina, T., Lammers, M., Toth, P., Charnikhova, T., de Maagd, R., Pozo, M.J., Bouwmeester, H., & Ruyter-Spira, C. (2012). The tomato CAROTENOID CLEAVAGE DIOXYGENASE8 (SlCCD8) is regulating rhizosphere signaling, plant architecture and reproductive development through strigolactone biosynthesis. *New Phytologist* 196(2), 535–547

Liu, H., Ding, Y., Zhou, Y., Jin, W., Xie, K., & Chen, L. L. (2017). CRISPR-P 2.0: An Improved CRISPR-Cas9 Tool for Genome Editing in Plants. *Molecular Plant* 10(3), 530–532

López-Gresa, M. P., Lisón, P., Campos, L., Rodrigo, I., Rambla, J. L., Granell, A., Conejero, V., & Bellés, J. M. (2017). A non-targeted metabolomics approach unravels the VOCs associated with the tomato immune response against Pseudomonas syringae. *Frontiers in Plant Science*, 8, 1188-1199.

López-Gresa, M. P., Payá, C., Ozáez, M., Rodrigo, I., Conejero, V., Klee, H., Bellés, J. M., & Lisón, P. (2018). A new role for green leaf volatile esters in tomato stomatal defense against pseudomonas syringe pv. Tomato. *Frontiers in Plant Science*, 9, 1855-1869.

López-Ráez, J. A., Matusova, R., Cardoso, C., Jamil, M., Charnikhova, T., Kohlen, W., Carolien, R. S., Verstappen, F., & Bouwmeester, H. (2009). Strigolactones: Ecological significance and use as a target for parasitic plant control. *Pest Management Science* 65(5), 471–477.

Matthys, C., Walton, A., Struk, S., Stes, E., Boyer, F. D., Gevaert, K., & Goormachtig, S. (2016). The Whats, the Wheres and the Hows of strigolactone action in the roots. *Planta* 243(6), 1327–1337.

McQuinn, R. P., Gapper, N. E., Gray, A. G., Zhong, S., Tohge, T., Fei, Z., Fernie, A. R., & Giovannoni, J. J. (2020). Manipulation of ZDS in tomato exposes carotenoid- and ABA-specific effects on fruit development and ripening. *Plant Biotechnology Journal*, 18(11), 2210–2224.

Moreno, J. C., Mi, J., Alagoz, Y., & Al-Babili, S. (2021). Plant apocarotenoids: from retrograde signaling to interspecific communication. *The Plant Journal*, 105(2), 351–375.

Nakahara, H., Mori, T., Sadakari, N., Matsusaki, H., & Matsuzoe, N. (2016). Biological control of the bacterial wilt of the tomato “Micro-Tom” by phenotypic conversion mutants of ralstonia solanacearum. *Environmental Control in Biology*, 54(3), 139–145.

Nouri, E., Surve, R., Bapaume, L., Stumpe, M., Chen, M., Zhang, Y., Ruyter-Spira, C., Bouwmeester, H., Glauser, G., Bruisson, S., & Reinhardt, D. (2021). Phosphate Suppression of Arbuscular Mycorrhizal Symbiosis Involves Gibberellic Acid Signaling. *Plant and Cell Physiology*, 62(6), 959–970.

Pino, L.E., Lima, J.E., Vicente, M.H., de Sá, A.F.L., Pérez-Alfocea, F., Albacete, A., Costa, J.L., Werner, T., Schmülling, T., Freschi, L., Figueira, A., Zsögön, A., Peres, L.E.P. (2022). Increased branching independent of strigolactone in cytokinin oxidase 2-overexpressing tomato is mediated by reduced auxin transport. *Molecular Horticulture* 2, 12.

Pulido, P., Perello, C., & Rodriguez-Concepcion, M. (2012). New Insights into Plant Isoprenoid Metabolism. *Molecular Plant*, 5(5), 964–967.

Rodriguez-Concepcion, M., Avalos, J., Bonet, M. L., Boronat, A., Gomez-Gomez, L., Hornero-Mendez, D., Limon, M. C., Meléndez-Martínez, A. J., Olmedilla-Alonso, B., Palou, A., Ribot, J., Rodrigo, M. J., Zacarias, L., & Zhu, C. (2018). A global perspective on carotenoids: Metabolism, biotechnology, and benefits for nutrition and health. *Progress in Lipid Research* 70, 62–93.

Ruiz-Lozano, J. M., Aroca, R., Zamarreño, Á. M., Molina, S., Andreo-Jiménez, B., Porcel, R., García-Mina, J. M., Ruyter-Spira, C., & López-Ráez, J. A. (2016). Arbuscular mycorrhizal symbiosis induces strigolactone biosynthesis under drought and improves drought tolerance in lettuce and tomato. *Plant Cell and Environment*, 39(2), 441–452.

Ruiz-Sola, M. Á., Barja, M. V., Manzano, D., Llorente, B., Schipper, B., Beekwilder, J., & Rodriguez-Concepcion, M. (2016a). A single arabidopsis gene encodes two differentially targeted geranylgeranyl diphosphate synthase isoforms. *Plant Physiology*, 172(3), 1393–1402.

Ruiz-Sola, M. Á., Coman, D., Beck, G., Barja, M. V., Colinas, M., Graf, A., Welsch, R., Rütimann, P., Bühlmann, P., Bigler, L., Gruissem, W., Rodríguez-Concepción, M., & Vranová, E. (2016b). Arabidopsis GERANYLGERANYL DIPHOSPHATE SYNTHASE 11 is a hub isozyme required for the production of most photosynthesis-related isoprenoids. *New Phytologist*, 209(1), 252-64

Ruiz-Sola, M. Á., & Rodríguez-Concepción, M. (2012). Carotenoid Biosynthesis in Arabidopsis: A Colorful Pathway. *The Arabidopsis Book*, 10, e0158.

Ruyter-Spira, C., Al-Babili, S., van der Krol, S., & Bouwmeester, H. (2013). The biology of strigolactones. *Trends in Plant Science* 18(2), 72–83.

Ruyter-Spira, C., Kohlen, W., Charnikhova, T., van Zeijl, A., van Bezouwen, L., de Ruijter, N., Cardoso, C., Lopez-Raez, J.A., Matusova, R., Bours, R., Verstappen, F., & Bouwmeester, H. (2011). Physiological effects of the synthetic strigolactone analog GR24 on root system architecture in Arabidopsis: Another below-ground role for strigolactones? *Plant Physiology* 155(2), 721–734.

Schilmiller, A. L., Schauvinhold, I., Larson, M., Xu, R., Charbonneau, A. L., Schmidt, A., Wilkerson, C., Last, R. L., & Pichersky, E. (2009). Monoterpenes in the glandular trichomes of tomato are synthesized from a neryl diphosphate precursor rather than geranyl diphosphate. *Proceedings of the National Academy of Sciences*, 106(26), 10865-10870.

Schuurink R, Tissier A. (2020). Glandular trichomes: micro-organs with model status*? New Phytologist*, 225(6), 2251-2266.

Simon, P. (2003). Q-Gene: Processing quantitative real-time RT-PCR data. *Bioinformatics*, 19(11), 1439–1440.

Stauder, R., Welsch, R., Camagna, M., Kohlen, W., Balcke, G. U., Tissier, A., & Walter, M. H. (2018). Strigolactone levels in dicot roots are determined by an ancestral symbiosis-regulated clade of the PHYTOENE SYNTHASE gene family. *Frontiers in Plant Science*, 9, 255-271.

Takahashi, H., Shimizu, A., Arie, T., Rosmalawati, S., Fukushima, S., Kikuchi, M., Hikichi, Y., Kanda, A., Takahashi, A., Kiba, A., Ohnishi, K., Ichinose, Y., Taguchi, F., Yasuda, C., Kodama, M., Egusa, M., Masuta, C., Sawada, H., Shibata, D., & Watanabe, Y. (2005). Catalog of Micro-Tom tomato responses to common fungal, bacterial, and viral pathogens. *Journal of General Plant Pathology*, 71(1), 8–22.

Tholl, D. (2015). Biosynthesis and Biological Functions of Terpenoids in Plants. *Advances in biochemical engineering/biotechnology* 148, 63–106.

Thulasiram, H. v., & Poulter, C. D. (2006). Farnesyl diphosphate synthase: The art of compromise between substrate selectivity and stereoselectivity. *Journal of the American Chemical Society*, 128(49), 15819–15823.

Ueda, H., & Kusaba, M. (2015). Strigolactone regulates leaf senescence in concert with ethylene in arabidopsis. *Plant Physiology*, 169(1), 138–147.

Visentin, I., Vitali, M., Ferrero, M., Zhang, Y., Ruyter-Spira, C., Novák, O., Strnad, M., Lovisolo, C., Schubert, A., & Cardinale, F. (2016). Low levels of strigolactones in roots as a component of the systemic signal of drought stress in tomato. *New Phytologist*, 212(4), 954–963.

Vogel, J. T., Walter, M. H., Giavalisco, P., Lytovchenko, A., Kohlen, W., Charnikhova, T., Simkin, A. J., Goulet, C., Strack, D., Bouwmeester, H. J., Fernie, A. R., & Klee, H. J. (2010). SlCCD7 controls strigolactone biosynthesis, shoot branching and mycorrhiza-induced apocarotenoid formation in tomato. *The Plant Journal*, 61(2), 300–311.

Wang, Q., Huang, X. Q., Cao, T. J., Zhuang, Z., Wang, R., & Lu, S. (2018). Heteromeric Geranylgeranyl Diphosphate Synthase Contributes to Carotenoid Biosynthesis in Ripening Fruits of Red Pepper (Capsicum annuum var. conoides). *Journal of Agricultural and Food Chemistry*, 66(44), 11691–11700.

Wang, Y., Duran, H. G. S., van Haarst, J. C., Schijlen, E. G., Ruyter-Spira, C., Medema, M. H., Dong, L., & Bouwmeester, H. J. (2021). The role of strigolactones in P deficiency induced transcriptional changes in tomato roots. *BMC plant biology*, 21(1), 1-21.

Wang, Y., Durairaj, J., Duran, H. G. S, van Velzen, R., Flokova, K., Liao, C. Y., Chojnacka, A., MacFarlane, S., Schranz, M. E., Medema, M. H., van Dijk, A. D. J., Dong, L., & Bouwmeester, H. J. (2022). The tomato cytochrome P450 CYP712G1 catalyses the double oxidation of orobanchol en route to the rhizosphere signalling strigolactone, solanacol. *New Phytologist* 235(5), 1884-1899.

Xie, X., Yoneyama, K., & Yoneyama, K. (2010). The strigolactone story. *Annual Review of Phytopathology*, 48, 93–117.

Yamada, Y., Furusawa, S., Nagasaka, S., Shimomura, K., Yamaguchi, S., & Umehara, M. (2014). Strigolactone signaling regulates rice leaf senescence in response to a phosphate deficiency. *Planta*, 240(2), 399–408.

Yamada, Y., & Umehara, M. (2015). Possible roles of strigolactones during leaf senescence. *Plants* 4(3), 664–677.

Yoneyama, K., Xie, X., Sekimoto, H., Takeuchi, Y., Ogasawara, S., Akiyama, K., Hayashi, H., & Yoneyama, K. (2008). Strigolactones, host recognition signals for root parasitic plants and arbuscular mycorrhizal fungi, from Fabaceae plants. *New Phytologist*, 179(2), 484–494.

Zhang, M., Yuan, B., & Leng, P. (2009). The role of ABA in triggering ethylene biosynthesis and ripening of tomato fruit. *Journal of Experimental Botany*, 60(6), 1579–1588.

Zhang, Y., van Dijk, A. D. J., Scaffidi, A., Flematti, G. R., Hofmann, M., Charnikhova, T., Verstappen, F., Hepworth, J., van der Krol, S., Leyser, O., Smith, S. M., Zwanenburg, B., Al-Babili, S., Ruyter-Spira, C., & Bouwmeester, H. J. (2014). Rice cytochrome P450 MAX1 homologs catalyze distinct steps in strigolactone biosynthesis. *Nature Chemical Biology*, 10(12), 1028–1033.

Zhou, F., & Pichersky, E. (2020). The complete functional characterisation of the terpene synthase family in tomato. *New Phytologist*, 226(5), 1341–1360.

Figures

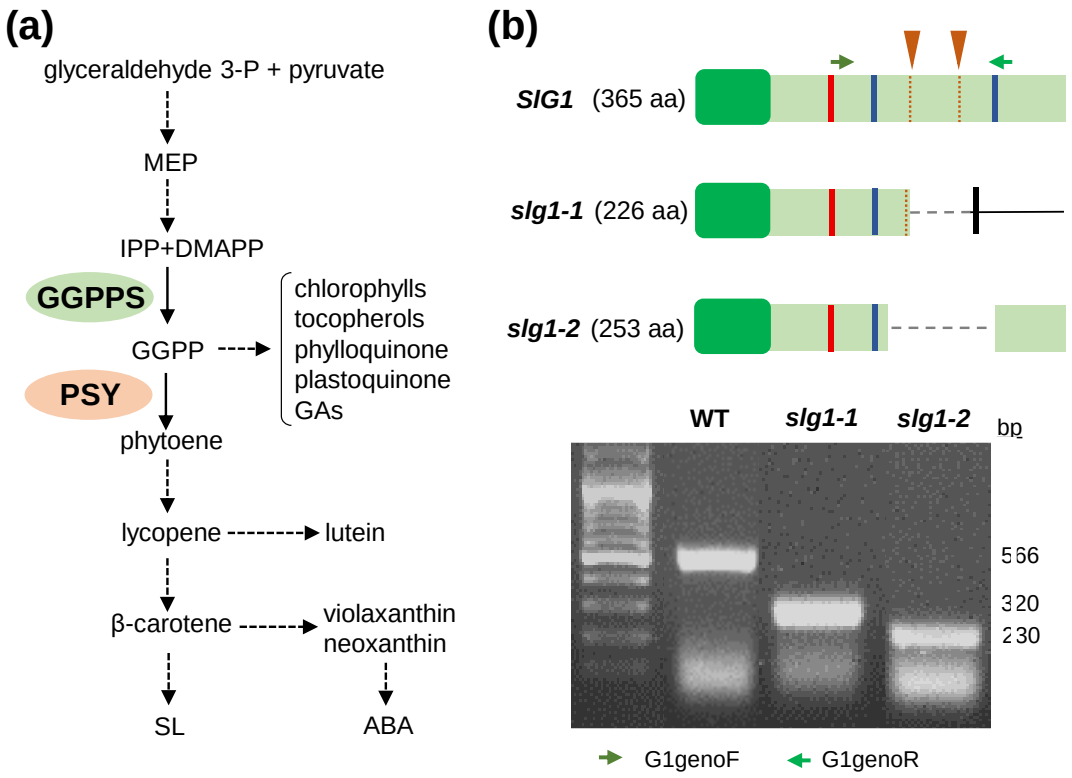

Figure 1. Carotenoid pathway and tomato mutants. (a) Carotenoid biosynthesis pathway. Dashed arrows represent multiple steps. The reactions catalyzed by geranylgeranyl diphosphate synthase (GGPPS) and phytoene synthase (PSY) are marked. **(b)** Scheme representing the wild-type SlG1 protein and the mutant versions generated in the corresponding CRISPR-Cas9-generated alleles (see Figure S1–S2 for further details). Dark green boxes represent plastid transit peptides. The regions targeted by the designed sgRNAs are indicated with orange arrowheads and dotted lines. Red and blue bars mark the position of conserved domains required for GGPPS activity (protein-protein interaction domains and Asp-rich domains, respectively). Deletions are shown with a dashed line. Green arrows represent the position of primers for PCR-based genotyping. The agarose gel shows the PCR genotyping products using these primers.

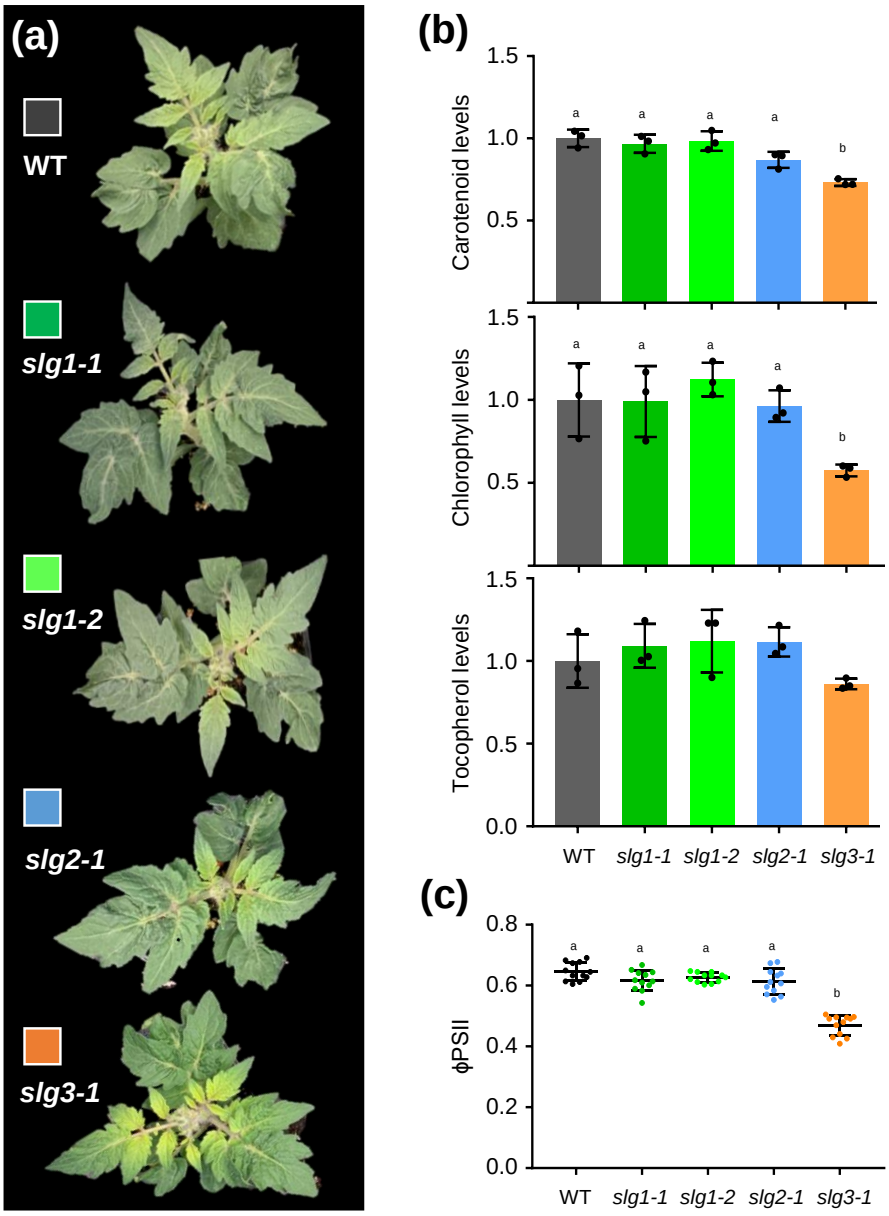

Figure 2. SlG1 does not contribute to GGPP-derived isoprenoid biosynthesis in tomato leaves. (a) Representative images of 4-week-old plants of WT and GGPPS-defective mutants. **(b)** Carotenoid, chlorophyll and tocopherol levels in young leaves from 4-week-old WT and mutant plants. Values are represented relative to WT levels and they correspond to mean and SD of n≥3 independent biological replicates. **(c)** Effective quantum yield of photosystem II (ϕPSII) in young leaves like those used in (b). Individual values (colored dots) and well as mean and SD are shown, and they correspond to four different areas from leaves of three different plants. In all plots, letters represent statistically significant differences ($P < 0.05$) among means according to post hoc Tukey's tests run when one way ANOVA detected different means.

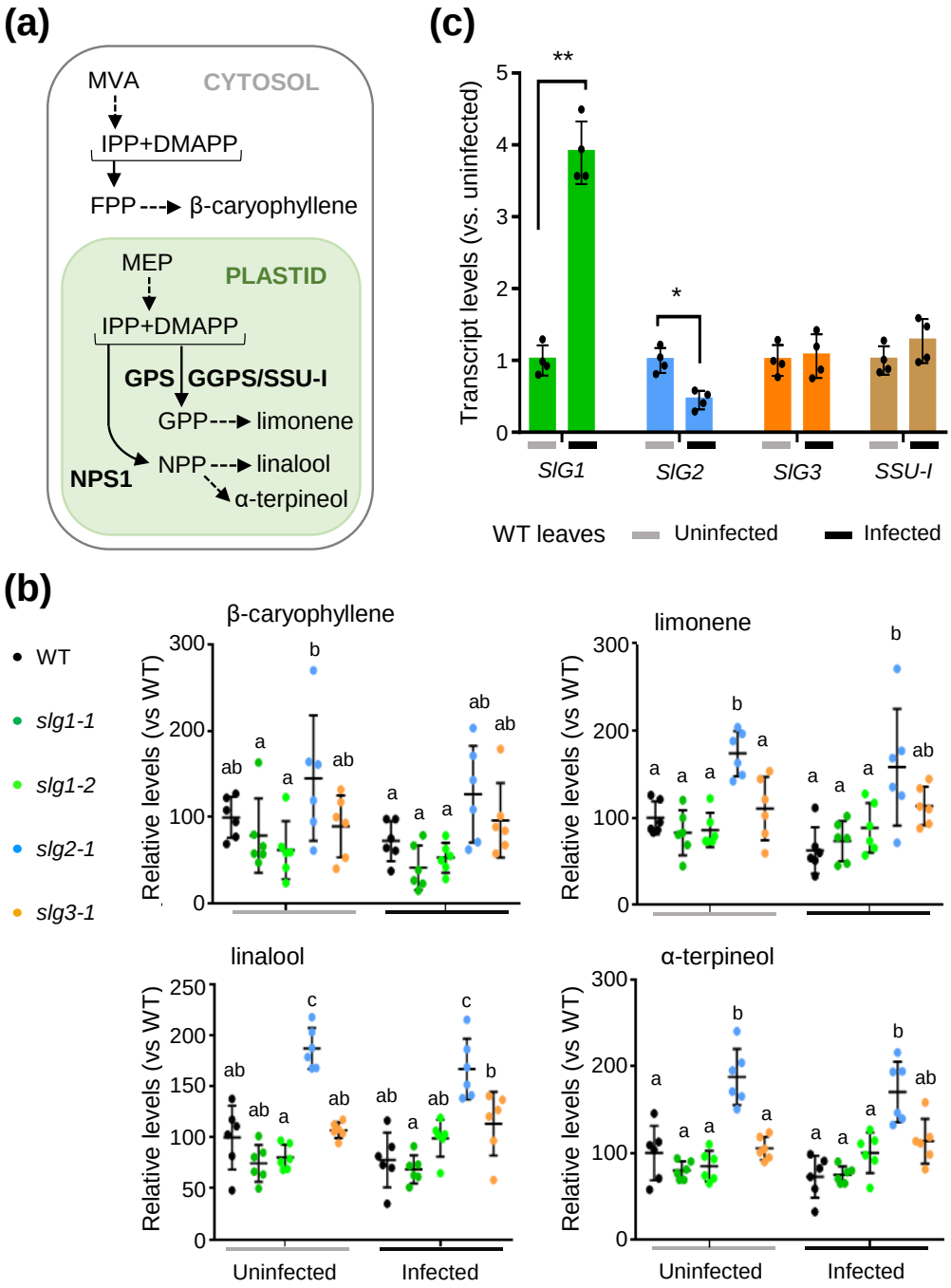

Figure 3. SlG1 is not required for monoterpene production in leaves. MicroTom WT and edited plants were infected with *Pseudomonas syringae pv. tomato* DC3000 and samples were collected 24 h later. **(a)** Biosynthetic pathways. **(b)** Levels of representative VOCs in infected and uninfected leaves of WT and GGPPS-defective mutants. Data are represented relative to the levels in uninfected WT samples (100%) and correspond to the mean ± SD of n=6 biological replicates. Letters represent statistically significant differences (one-way ANOVA followed by Tukey's multiple comparisons test, $P < 0.05$). A schematic representation of the VOC biosynthesis pathway is shown in the left side. **(c)** RT-qPCR expression data of the indicated genes in WT leaves. Expression levels are shown relative to uninfected samples and they correspond to the mean ± SD of n=4 independent biological replicates. Asterisks indicate statistically significant differences among means between uninfected and infected samples (t-test: *, $P < 0.05$; **, $P < 0.01$).

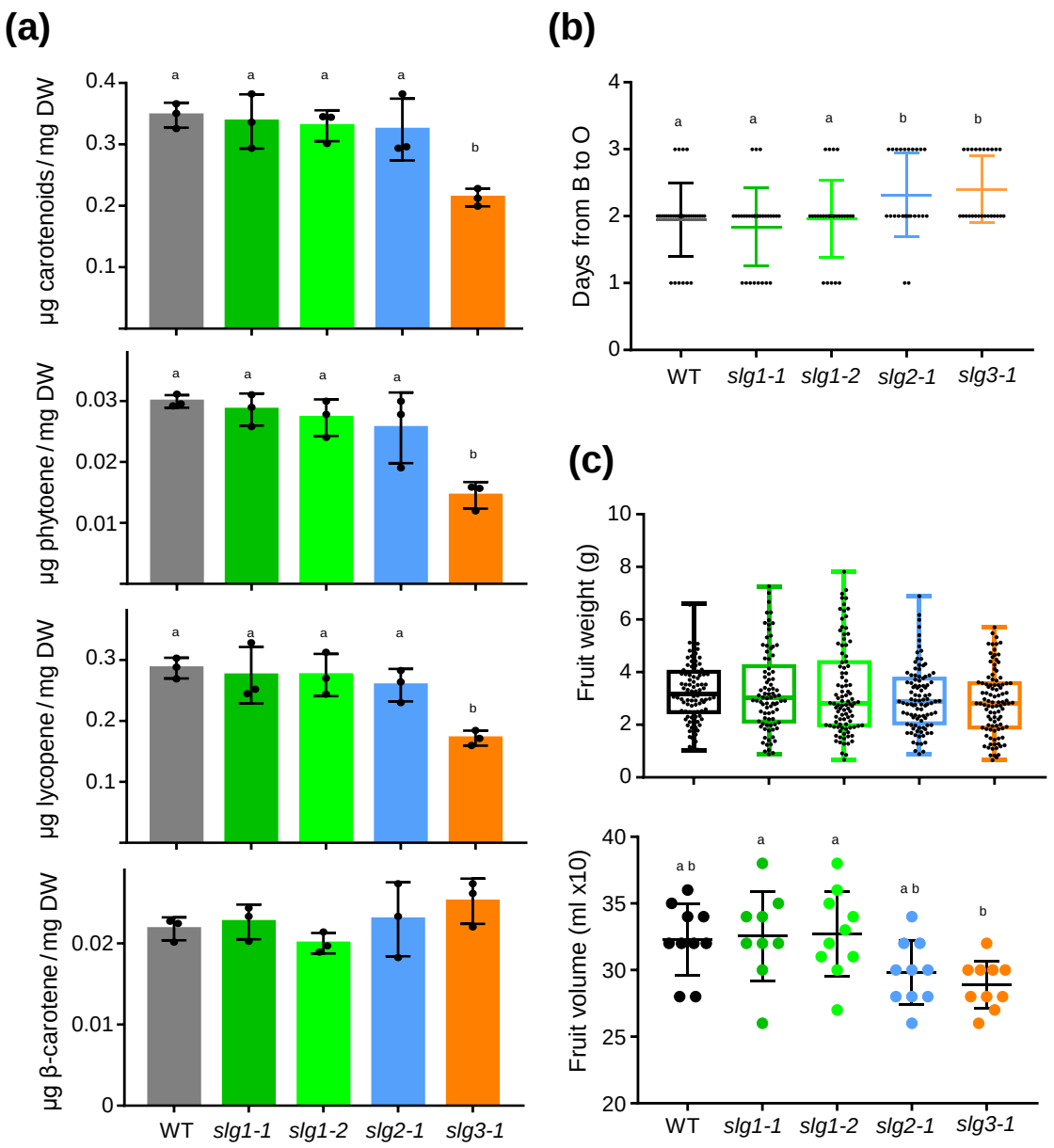

Figure 4. SlG1 is dispensable for carotenoid biosynthesis in fruits. (a) Levels of total and individual carotenoids (phytoene, lycopene and β-carotene) in tomato fruits collected from the plant 3 days after the breaker stage (B+3) fruits. Values represent mean and SD of n=3 independent biological replicates**. (b)** Fruit ripening rate estimated as the number of days from B to O stages in the plant. Black dots indicate individual values and colored lines represent the mean and the SD. **(c)** Weight and volume of fully ripe (R) fruits of the indicated genotypes. In the weight boxplot, the lower and upper boundary of the boxes indicate the 25th and 75th percentile, respectively; the line inside the boxes represents the median; dots mark individual data values; and whiskers above and below the boxes indicate the maximum and minimum values. In the volume dotplot, central line represents the mean and whiskers represent SD. In all cases, letters represent statistically significant differences ($P < 0.05$) among means according to post hoc Tukey's tests run when one way ANOVA detected different means.

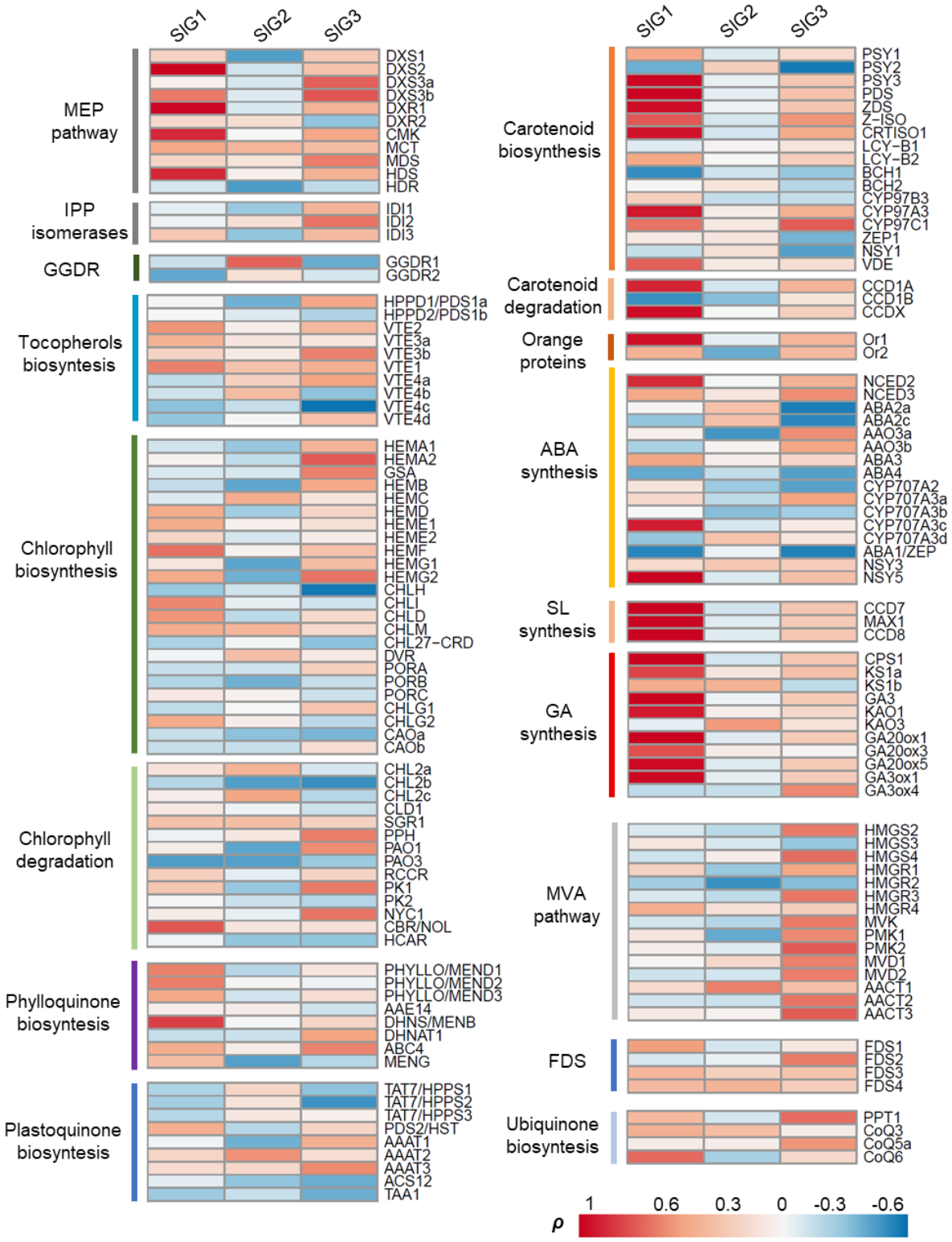

Figure 5. *SIG1* expression is highly connected with carotenoid and SL biosynthesis in roots. Heatmap represents pairwise Pearson correlations (ρ) between the expression of genes encoding GGPPS isoforms and those for the indicated enzymes from pathways upstream and downstream of GGPP. Gene details, abbreviations, accessions, and data correlations are listed in Table S3.

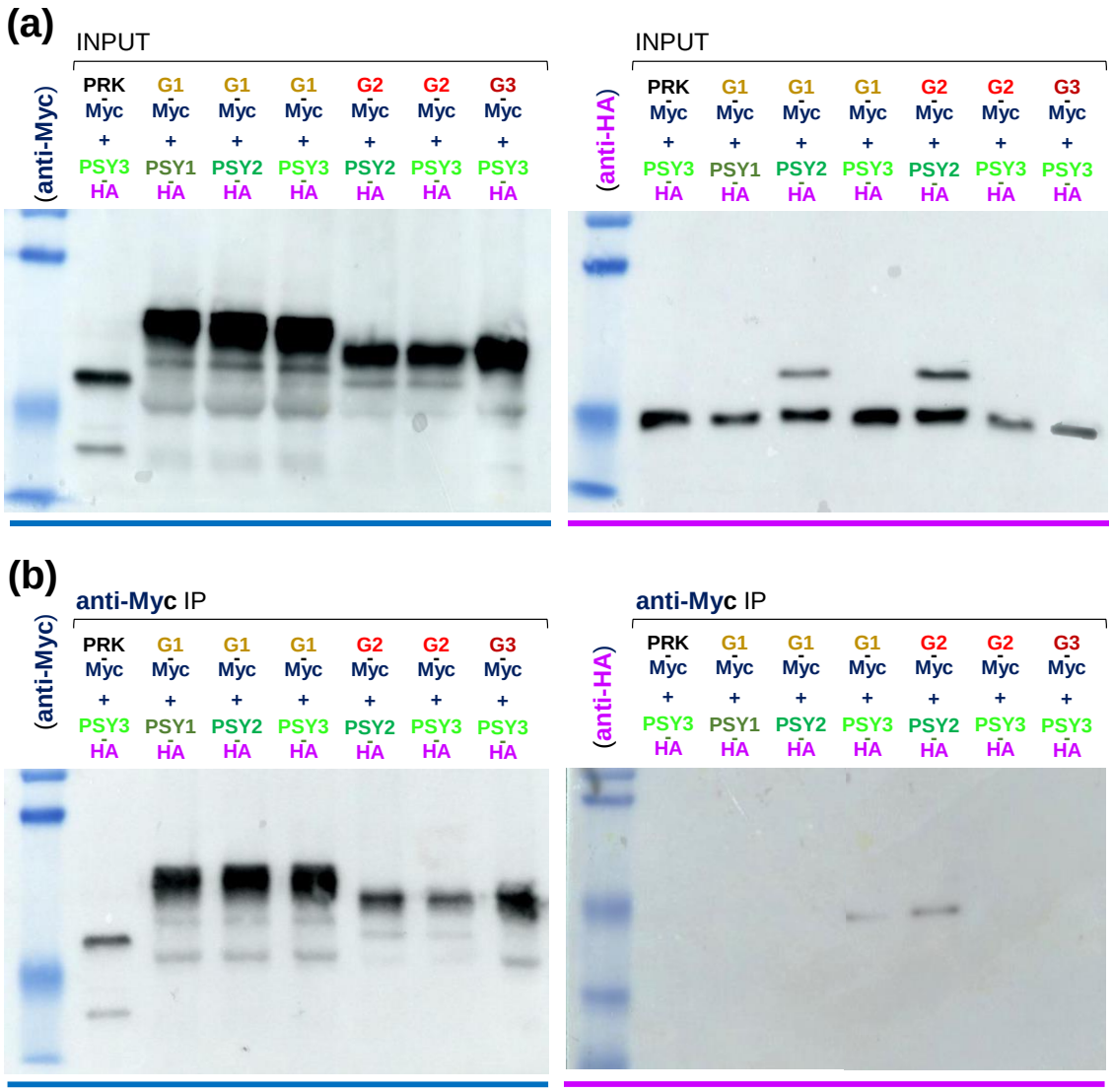

Figure 6. SlG1 specifically interacts with PSY3 *in planta*. *N. benthamiana* leaves were co-agroinfiltrated with constructs encoding the indicated proteins tagged with C-terminal Myc or HA epitopes. **(a)** Immunoblot analysis of crude extracts (INPUT) with anti-Myc (dark blue) and anti-HA (purple) antibodies to confirm successful protein production. **(b)** Immunoblot analysis of extracts after immunoprecipitation (IP) with anti-Myc. The same samples were used for immunodetection with anti-Myc (to confirm successful IP) or anti-HA (to identify co-immunoprecipitated partners). Predicted protein molecular weights (KDa): PRK-Myc, 52.1; SlG1-Myc, 56.9; SlG2-Myc, 55.3; SlG3-Myc, 55.5; PSY1-HA, 50.7; PSY2-HA, 51.0; PSY3-HA, 50.2.

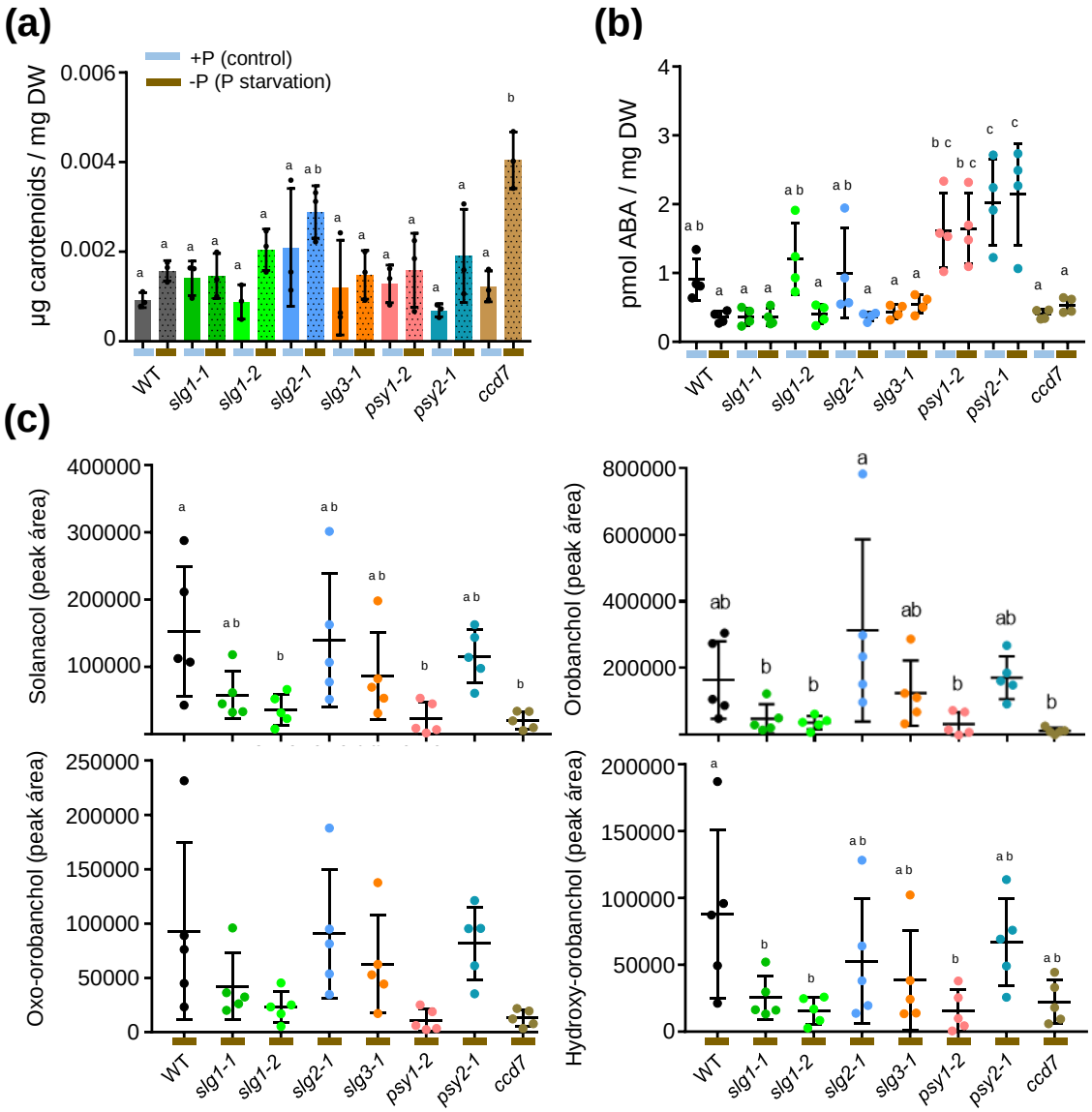

Figure 7. SlG1 is involved in root SL production. Plants of the indicated genotypes were grown in half-strength Hoagland solution with normal phosphate (+P) or under phosphate starvation (-P) conditions. Samples of root tissues or exudates were collected for metabolite analyses. **(a)** Carotenoid levels in root tissues. Values correspond to the mean and SD of n≥3 independent biological replicates. **(b)** ABA levels in root tissues. Values correspond to mean and SD of n≥4 independent biological replicates. **(c)** Levels of individual SLs in root exudates. Values represent the mean and SD of n≥5 independent biological replicates. In dotplots, inner line is the mean and whiskers represent SD. In all cases, letters represent statistically significant differences ($p<0.05$) among means according to posthoc Tukey's tests run when one-way ANOVA detected different means.

Solanacol

Orobanchol

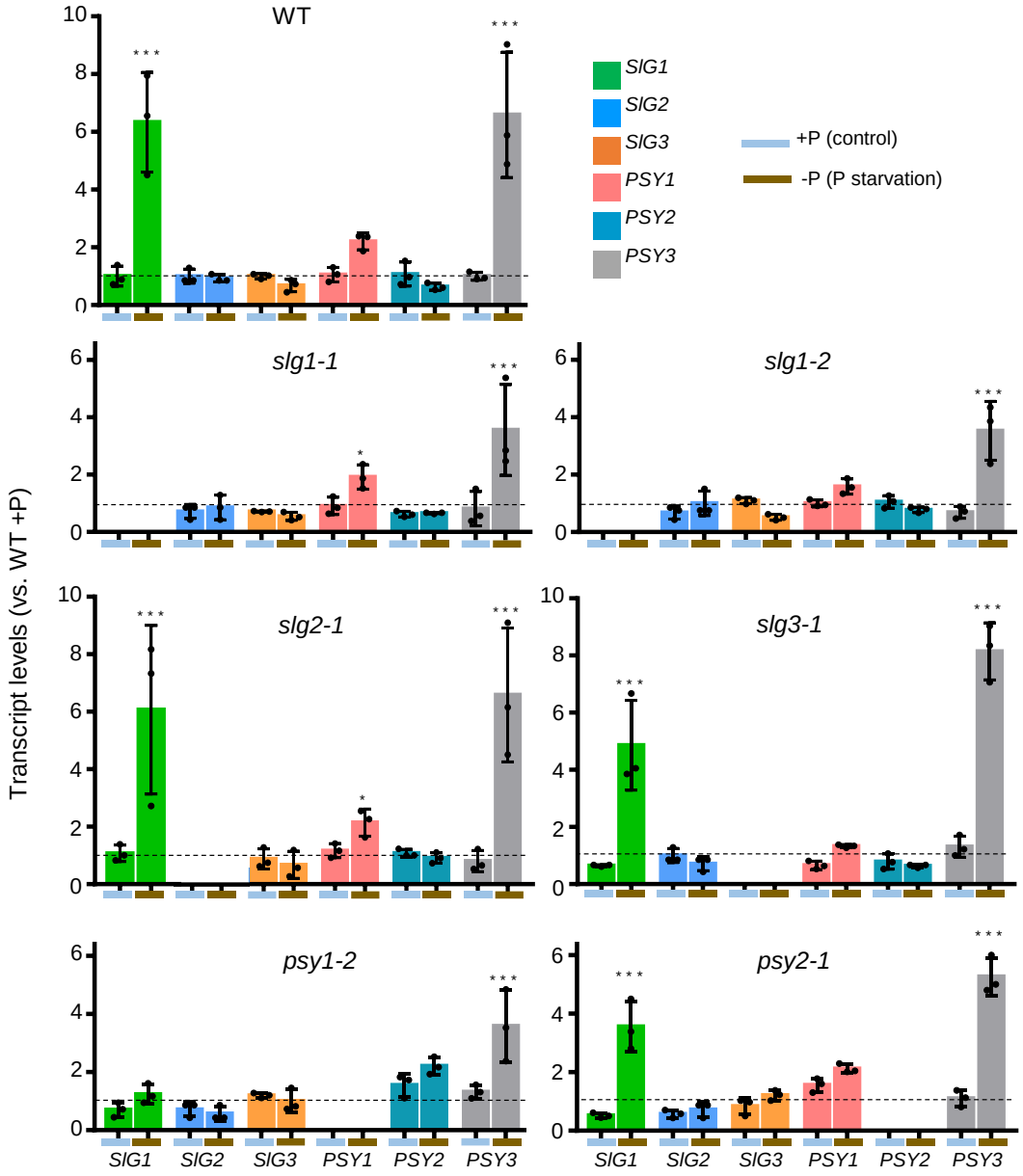

Figure 8. Genes encoding GGPPS and PSY paralogues show differential responses to phosphate starvation in roots. RNA samples from roots collected from the plants described in Figure 7 were used for RT-qPCR experiments. Transcript levels were normalized using the tomato *ACT4* gene and they are shown relative to those in control (+P) WT samples (dotted line). The scale is the same in all plots to facilitate comparisons. Mean and SD of n=3 independent biological replicates are shown. Asterisks indicate statistically significant differences between conditions (+P vs -P) for each gene in each genotype according to one-way ANOVA with Dunnett's multiple comparisons test: *, $P < 0.05$; **, $P < 0.01$; ***, $P < 0.001$).

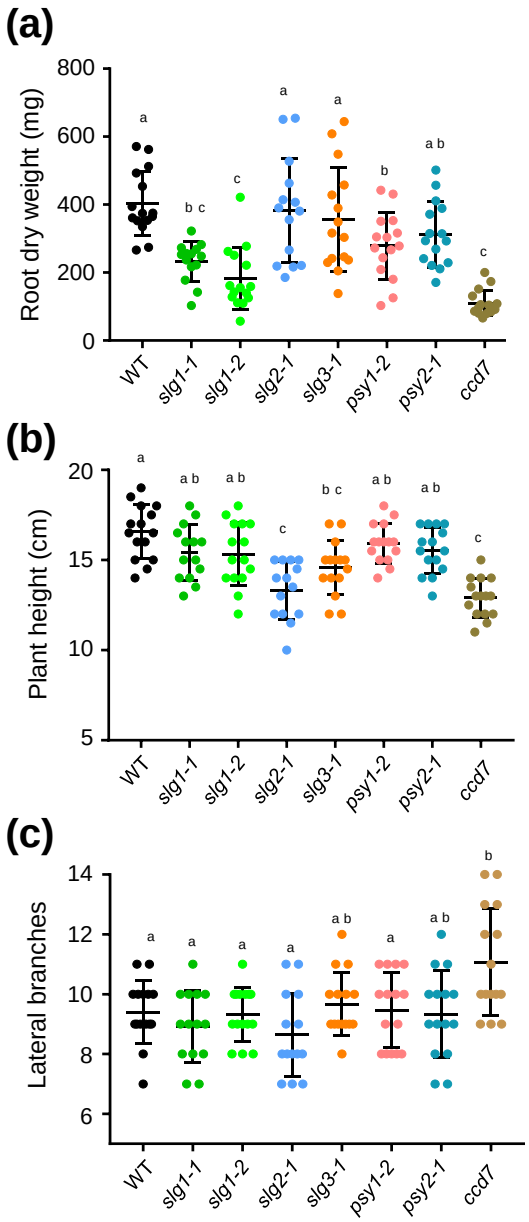

Figure 9. Defective SL synthesis in *slg1* plants does not impact shoot growth or branching. Measurements were performed using plants of the indicated genotypes grown under +P for 4 weeks and then transferred to -P for 2 more week to promote SL synthesis. **(a)** Weight of entire roots after freeze-drying. **(b)** Plant height from the root-stem transition to the apical meristem bud. **(c)** Number of lateral branches arising from the main stem. In all plots, dots indicate individual values, whiskers indicate mean and SD, and letters represent statistically significant differences ($P < 0.05$) among means according to posthoc Tukey's tests run when one-way ANOVA detected different means.

752

Supporting information

SUPPORTING METHODS

Methods S1. Metabolite analyses.

Isoprenoid extraction and quantification. Carotenoids, chlorophylls and tocopherols were extracted as described (Barja et al., 2021; Ezquerro et al., 2022) with some modifications. Freeze-dried tissue powder from roots (25 mg) or leaves (8 mg) was mixed in 2 ml Eppendorf tubes with 375 µl of methanol as extraction solvent, 25 µl of a 10 % (w/v) solution of canthaxanthin (Sigma) in chloroform as internal control, and three 2 mm glass beads. In the case of pericarp tissue, freeze-dried powder (20 mg) was 1 ml of 2:1:1 hexane:acetone:methanol was used instead of methanol. Following extraction as described (Barja et al., 2021; Ezquerro et al., 2022), dry residues were resuspended in 200 µl of acetone by using an ultrasound bath and filtered with 0.2 µm filters into amber-colored 2 ml glass vials. Separation and quantification of individual carotenoids, chlorophylls and tocopherols was performed as described (Barja et al., 2021).

ABA extraction and quantification. For ABA quantification, 20 mg of freeze-dried root powder was mixed using 1 ml of 10% methanol in water (containing internal ABA standard) by shaking in a TissueLyser II (Quiagen) at 27 Hz for 3 min. Next, samples were placed in a rotator for 1 hour at 4°C. Extracts were then centrifuged at 14000 x*g* at 4°C for 15 min. Around 800 µl of the liquid phase was recovered in 1.5 ml Eppendorf for further steps. Eluted liquid was run through an Oasis HLB (reverse phase) column as described (Flokova et al., 2014). The dry residues were dissolved in 1 ml of pure methanol and after, dried under a nitrogen flow in a fume hood for 40 min. The eluate was dissolved in 5% acetonitrile and ABA was detected using a reverse phase UHPLC chromatography. The gradient used contains 5 to 50% acetronitrile with 0.05% acetic acid, at a flow speed of 400 µL/min over 21 min. Quantification of ABA was perform with a Q-Exactive mass spectrometer (Orbitrap detector; ThermoFisher Scientific) in conjunction with internal standards (deuterium-labelled hormone at 1pmol/µl), calibration curves and the TraceFinder 4.1 SP1 software.

SL extraction and quantification. Tomato seedlings growing in a mixture of river sand and a clay granulate (1:1) were supplied with half-strength Hoagland solution twice a week for 28 days. After 28 days, plants were divided into two groups of which one continued to get the half-strength Hoagland solution for 7 days, while the other was exposed to phosphorus deficiency (by using half-strength Hoagland solutions without

phosphate) to induce SL biosynthesis and exudation. Pots were washed with 100 ml of sterile mili-Q water to collect the SLs, which were then concentrated using C18 SPE columns (SUPELCO, Discovery® DSC-18 SPE, 500 mg/3 mL) and analyzed by LC-MS/MS as described (Zhang et al., 2014; 2018).

Analysis of volatile organic compounds. For the analysis of VOCs, frozen tomato leaf powder (150 mg) was mixed in a 15 ml glass vial with 1 mL of a saturated $CaCl_2$ solution and 100 µL of 750 mM EDTA (pH 7.5). The vial was sealed and sonicated for 5 min and volatile compounds extraction was performed by Head Space Solid-Phase Microextraction (HS-SPME) as previously reported (López-Gresa et al., 2017). VOCs were analyzed in an Agilent 6890N (Santa Clara, CA, USA) gas chromatograph coupled to an Agilent 5975B Inert XL electronic impact (EI) mass detector with an ionization energy of 70 eV and a source temperature of 230°C. Chromatograms were processed using the Enhanced ChemStation software (Agilent). Final identification of VOCs was performed using commercial standards as reported (López-Gresa et al., 2018).

Methods S2. Gene expression analyses.

Gene co-expression network (GCN) analyses. The data set used for Gene co-expression network construction was previously described (Wang et al., 2021) and it is publicly available in https://dataview.ncbi.nlm.nih.gov/ object/ PRJNA 679261? reviewer=vs5lk 0a94j04c2rgieta1lrlro. It is composed by tomato root samples grown in +P and -P conditions. Tomato isoprenoid biosynthetic genes were retrieved from Plaza 4.0 using Arabidopsis homologs as queries (https://bioinformatics.psb.ugent.be/plaza/) as previously described (Wang et al., 2022). Pairwise pearson correlation coefficients (PCC) were calculated between every two genes using *SlG1*, *SlG2* and *SlG3* as baits and tomato isoprenoid biosynthetic genes as preys. Figures were constructed using R software (https://www.r-project.org/).

RNA extraction and RT-qPCR analyses. Total RNA from freeze-dried leaves and roots was extracted using TriPure isolation reagent (Sigma) combined with a Qiagen RNeasy mini spin column kit following manufacturer's instructions. RNA was quantified using a NanoDropTM 8000 spectrophotometer (ThermoFisher Scientific). ThermoFisher First Strand cDNA synthesis kit using oligo(dT) primer was used to reverse transcribe 1000 ng of RNA into 20 µL of cDNA, which was subsequently diluted 10-fold with mili-Q water and stored at -20 °C for further analysis. Relative mRNA abundance was evaluated via Real-Time Quantitative Polymerase Chain Reaction (RT-qPCR) in a

reaction volume of 10 µL containing 5 µL of SYBR Green Master Mix (Thermo Fisher Scientific), 0.3 µM of each specific forward and reverse primer (Table S1) and 2 µL of cDNA. Transcript abundance was evaluated via real-time quantitative PCR (RT-qPCR) in a reaction volume of 10 µl containing 2 µl of the cDNA dilution, 5 µl of SYBR Green Master Mix (Thermo Fisher Scientific), and 0.3 µM of each specific forward and reverse primer (Table S1). The RT-qPCR was carried out on a QuantStudio 3 Real-Time PCR System (Thermo Fisher Scientific) using three independent biological samples and three technical replicates of each sample. Normalized transcript abundance was calculated as previously described (Simon, 2003) using tomato *ACT4* (Solyc04g011500) as endogenous reference gene.

Methods S3. Co-immunoprecipitation assays.

Co-immunoprecipitation experiments were carried out as described (Barja & Rodríguez-Concepción, 2020; Barja et al., 2021) (Methods S3). Constructs encoding Myc- and HA-tagged tomato GGPPS and PSY proteins (Table S2) (Barja et al., 2021) were transformed into *A. tumefaciens* GV3101 strains. A plasmid containing the Arabidopsis phosphoribulokinase protein with a Myc tag (pGWB417_PRK-Myc) was used as negative control. Agroinfiltration of *N. benthamiana* leaves, sample collection, protein extraction and immunoprecipitation of proteins was performed as described (Barja et al., 2021). Myc- and HA-tagged proteins in input and Co-IP samples were detected by immunoblot analyses using 1:2000 αMyc (Sigma) and 1:1000 αHA (Roche) dilutions. Horseradish peroxidase (HRP)-conjugated secondary antibodies against mouse and rat IgGs, respectively were used in a 1:10000 dilution. Amersham ECL Prime Western Blotting Detection Kit (GE Healthcare) was used for detection and the signal was visualized using the Amersham ImageQuant 800 Western blot imaging system.

SUPPORTING FIGURES

```
SLG1      ACGAAGGCAATCAAGGTAAACAAAGCACTAGATGAAGCAATACCAATGCAAGAGCCTATA 300
slg1-1    ACGAAGGCAATCAAGGTAAACAAAGCACTAGATGAAGCAATACCAATGCAAGAGCCTATA 300
slg1-2    ACGAAGGCAATCAAGGTAAACAAAGCACTAGATGAAGCAATACCAATGCAAGAGCCTATA 300
          ************************************************************

SLG1      AAAGTTCATGAAGCCATGAGGTACTCACTTCTAGCTGGAGGAAAACGTGTCCGGCCGATC 360
slg1-1    AAAGTTCATGAAGCCATGAGGTACTCACTTCTAGCTGGAGGAAAACGTGTCCGGCCGATC 360
slg1-2    AAAGTTCATGAAGCCATGAGGTACTCACTTCTAGCTGGAGGAAAACGTGTCCGGCCGATC 360
          ************************************************************

SLG1      CTCTGCATGGCTTCTTGTGAAGTTGTAGGAGGGGATGAATCCTTAGCTATACCTGCAGCT 420
slg1-1    CTCTGCATGGCTTCTTGTGAAGTTGTAGGAGGGGATGAATCCTTAGCTATACCTGCAGCT 420
slg1-2    CTCTGCATGGCTTCTTGTGAAGTTGTAGGAGGGGATGAATCCTTAGCTATACCTGCAGCT 420
          ************************************************************
          G1 CRISPR Geno F
SLG1      TGCGCAGTTGAGATGATCCATACCATGTCACTCGTCCATGATGATCTTCCCTGCATGGAC 480
slg1-1    TGCGCAGTTGAGATGATCCATACCATGTCACTCGTCCATGATGATCTTCCCTGCATGGAC 480
slg1-2    TGCGCAGTTGAGATGATCCATACCATGTCACTCGTCCATGATGATCTTCCCTGCATGGAC 480
          ************************************************************

SLG1      AACGATGATCTACGTCGTGGCAAGCCCACGAACCATAAGGTTTTTGGAGAAAACACTGCA 540
slg1-1    AACGATGATCTACGTCGTGGCAAGCCCACGAACCATAAGGTTTTTGGAGAAAACACTGCA 540
slg1-2    AACGATGATCTACGTCGTGGCAAGCCCACGAACCATAAGGTTTTTGGAGAAAACACTGCA 540
          ************************************************************

SLG1      GTTCTTGCAGGGGATGCACTTTTATCTTTGGCCTTTGAACATGTGGCTACCAAGACTCAG 600
slg1-1    GTTCTTGCAGGGGATGCACTTTTATCTTTGGCCTTTGAACATGTGGCTACCAAGACTCAG 600
slg1-2    G-----------------------------------------------------------  541
          *
                                                        sgRNA-1
SLG1      AATGTGCCACCCCAAAGAGTGGTCCAAGCCATTGGGGAATTGGGTTCAGCTGTTGGCTCA 660
slg1-1    AATGTGCCACCCCAAAGAGTGGTCCAAGCCATTGGGGAATTGGGTTCAGCTGTTGGCTCA 660
slg1-2    ------------------------------------------------------------541
            PAM
SLG1      GAAGGGCTCGTGGCAGGGCAAATTGTGGACTTGGCGAGTGAAGGAAAACAAGTTAGCCTA 720
slg1-1    GAAGGGCTCGTGGCAGG------------------------------------------- 677
slg1-2    ------------------------------------------------------------ 541

                        sgRNA-2      PAM
SLG1      ACTGAACTGGAGTACATTCACCACCATAAGACGGCGAAGCTTTTGGAGGCTGCTGTGGTT 780
slg1-1    ------------------------------------------------------------ 677
slg1-2    ------------------------------------------------------------ 541

SLG1      TGTGGGGCAATAATGGGGGGAGGAAATGAGGTTGATGTGGAGCGAATGAGGAGCTATGCT 840
slg1-1    ------------------------------------------------------------ 677
slg1-2    ------------------------------------------------------------ 541

SLG1      AGGTGCATTGGACTGTTATTTCAAGTGGTAGATGATATTCTTGATGTTACCAAGTCATCA 900
slg1-1    ------------------------------------------------------------ 677
slg1-2    -------------------------------------TTCTTGATGTTACCAAGTCATCA 569

SLG1      GATGAGCTGGGAAAGACAGCGGGTAAGGACCTAATAACAGATAAGGCTACATATCCTAAG 960
slg1-1    ----------------------GTAAGGACCTAATAACAGATAAGGCTACATATCCTAAG 715
slg1-2    GATGAGCTGGGAAAGACAGCGGGTAAGGACCTAATAACAGATAAGGCTACATATCCTAAG 644
                                ************************************
```

```
                                                                                                  ..........................................
                G1 CRISPR Geno R
SLG1       TTGATGGGGCTAGAAAAGGCTCGACAATATGCCGGTGAGCTGATGGCTAAGGCCATGAAT 1020
slg1-1     TTGATGGGGCTAGAAAAGGCTCGACAATATGCCGGTGAGCTGATGGCTAAGGCCATGAAT 775
slg1-2     TTGATGGGGCTAGAAAAGGCTCGACAATATGCCGGTGAGCTGATGGCTAAGGCCATGAAT 684
           ************************************************************

SLG1       GAGCTAAGCTACTTCGACTATGCAAAGGCAGCACCTCTTTATCATATTGCTAGTTATATT 1080
slg1-1     GAGCTAAGCTACTTCGACTATGCAAAGGCAGCACCTCTTTATCATATTGCTAGTTATATT 835
slg1-2     GAGCTAAGCTACTTCGACTATGCAAAGGCAGCACCTCTTTATCATATTGCTAGTTATATT 744
           ************************************************************

SLG1       GCAAATCGACAGAATTGA 1098
slg1-1     GCAAATCGACAGAATTGA 853
slg1-2     GCAAATCGACAGAATTGA 762
           ******************
```

Figure S1. DNA sequence alignment of *SlG1* CRISPR mutants. Alignment was performed using Clustal Omega (https://www.ebi.ac.uk/Tools/msa/clustalo/) with default settings. The sequence encoding the predicted plastid-targeting peptide is marked in green. Designed single-guide RNAs (sgRNA) are highlighted in blue and genotyping oligonucleotides are highlighted in fucsia. Protospacer adjacent motifs (PAM) are highlighted in red. Translation stop codons are underlined and marked in bold. Numbers at the end of each sequence indicate DNA sequence length.

```
                    Transit peptide
SlG1      MAFLATISGLDNLFLSNTPNNNFAFSRKLPPSQSYSFLHKKIHASDVANSFQTFQVKERD 60
slg1-1    MAFLATISGLDNLFLSNTPNNNFAFSRKLPPSQSYSFLHKKIHASDVANSFQTFQVKERD 60
slg1-2    MAFLATISGLDNLFLSNTPNNNFAFSRKLPPSQSYSFLHKKIHASDVANSFQTFQVKERD 60
          ************************************************************

SlG1      VSSKAEKFILPEFEFQEYMVTKAIKVNKALDEAIPMQEPIKVHEAMRYSLLAGGKRVRPI 120
slg1-1    VSSKAEKFILPEFEFQEYMVTKAIKVNKALDEAIPMQEPIKVHEAMRYSLLAGGKRVRPI 120
slg1-2    VSSKAEKFILPEFEFQEYMVTKAIKVNKALDEAIPMQEPIKVHEAMRYSLLAGGKRVRPI 120
          ************************************************************

           CxxxC                              FARM
SlG1      LCMASCEVVGGDESLAIPAACAVEMIHTMSLVHDDLPCMDNDDLRRGKPTNHKVFGENTA 180
slg1-1    LCMASCEVVGGDESLAIPAACAVEMIHTMSLVHDDLPCMDNDDLRRGKPTNHKVFGENTA 180
slg1-2    LCMASCEVVGGDESLAIPAACAVEMIHTMSLVHDDLPCMDNDDLRRGKPTNHKVFGENTA 180
          ************************************************************

                                          sgRNA-1
SlG1      VLAGDALLSLAFEHVATKTQNVPPQRVVQAIGELGSAVGSEGLVAGQIVDLASEGKQVSL 240
slg1-1    VLAGDALLSLAFEHVATKTQNVPPQRVVQAIGELGSAVGSEGLVAG*------------- 226
slg1-2    V------------------------------------------------------------ 181
          *
              sgRNA-2                                       SARM
SlG1      TELEYIHHHKTAKLLEAAVVCGAIMGGGNEVDVERMRSYARCIGLLFQVVDDILDVTKSS 300
slg1-1    ------------------------------------------------------------ 226
slg1-2    ---------------------------------------------------LDVTKSS 188

SlG1      DELGKTAGKDLITDKATYPKLMGLEKARQYAGELMAKAMNELSYFDYAKAAPLYHIASYI 360
slg1-1    ------------------------------------------------------------ 226
```

Figure S2. Protein alignments of SlG1 wild-type sequences with the selected CRISPR mutants. Multiple sequence alignment was performed using *Clustal Omega* (https://www.ebi.ac.uk/Tools/msa/clustalo/) with default settings**.** The predicted targeting peptides, the region of the designed sgRNAs and the catalytic motifs FARM (first aspartate-rich motif) and SARM (second-aspartate rich motif) are boxed in green, blue and black, respectively. The protein-protein interaction CxxxC (x = any hydrophobic residue) motifs are highlighted in pink. Numbers at the end of each sequence indicate protein length.

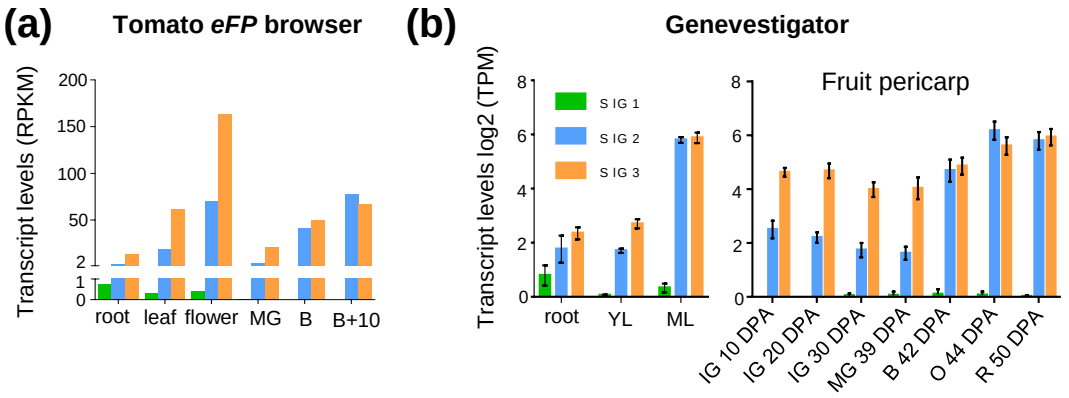

Figure S3. *SlG1, SlG2 and SlG3* transcript levels in different tissues and developmental stages. (a) RNAseq data retrieved from the *Tomato eFP Browser* database (http://bar.utoronto.ca/efp_tomato/cgi-bin/efpWeb.cgi). Levels are represented as RPKM (Reads per Kilobase of transcript per Million mapped reads). **(b)** RNAseq data obtained from Genevestigator (https://genevestigator.com). Levels are represented as log2 TPM (Transcripts Per Million mapped reads). Abbreviations: DPA, days post-anthesis; IG, immature green; MG, mature green; B, breaker; O, orange, R, red. YL, young leaves; ML, mature leaves.

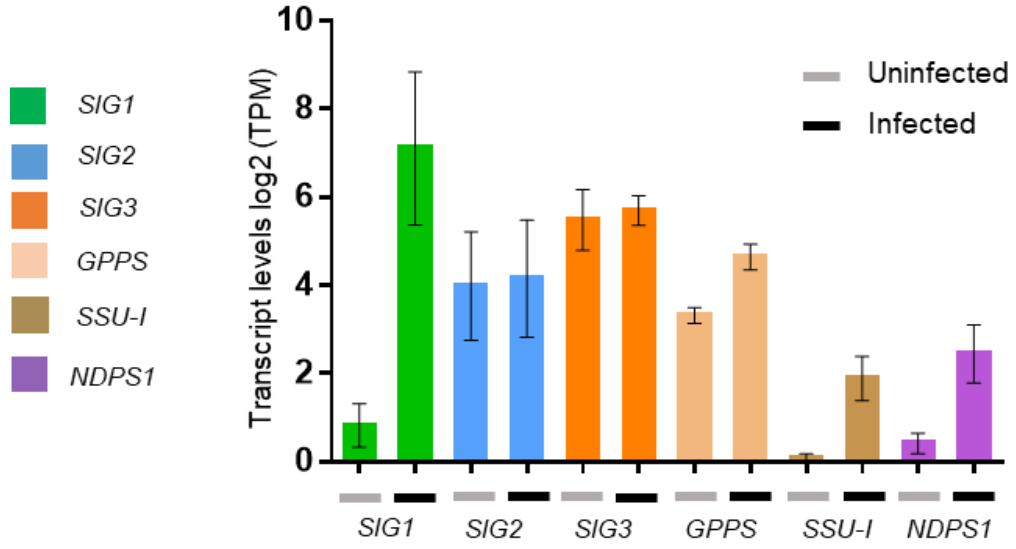

Figure S4. Expression levels of *SlGGPPS, SlGPPS, SlSSUI and SlNPS1* in leaves after *Pseudomonas syringae* infection. RNAseq data obtained from Genevestigator (https://genevestigator.com) of three different tomato infection experiments with *P.syringae pv. tomato* DC3000*.* Two different tomato cultivars were used, Ailsa Craig (Yang et al. 2016) and Rio Grande (Rosli et al., 2013; Pombo et al., 2014). Samples were collected at 9 (Ailsa Craig) or 6 (Rio Grande) hours post infection, respectively. Plots show the transcript levels of the indicated genes in leaves of both cultivars during *P. syringae pv. tomato* DC3000 infection and are shown as log2 TPM (Transcripts per Million mapped reads).

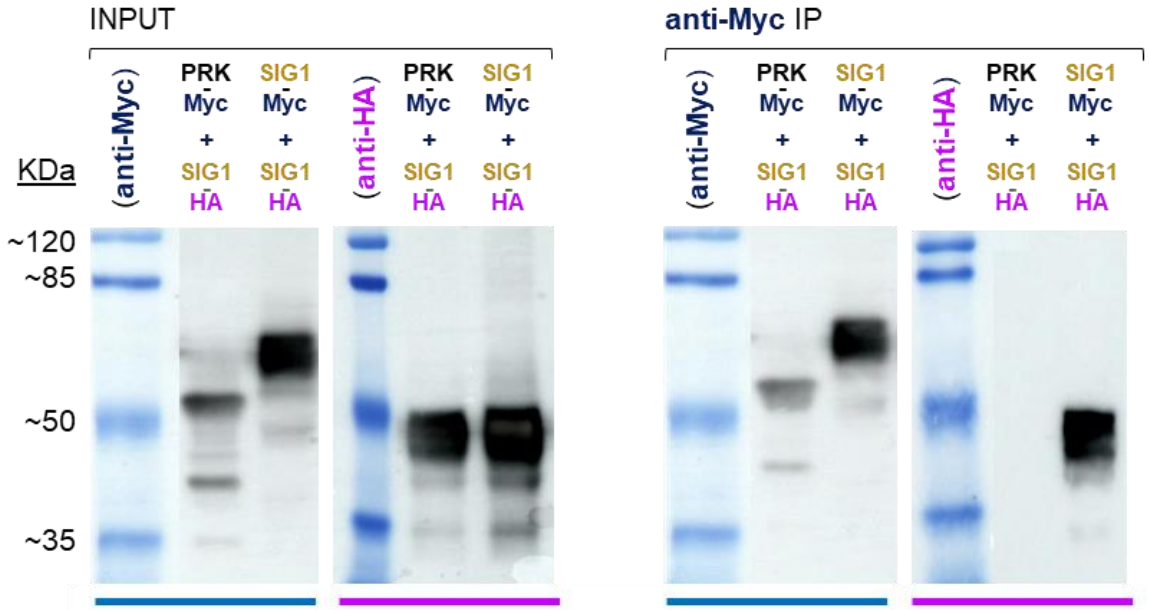

Figure S5. SlG1-Myc is able to specifically bind to protein partners. *N. benthamiana* leaves were co-agroinfiltrated with constructs encoding the indicated proteins tagged with C-terminal Myc or HA epitopes. Immunoblot analysis of crude extracts (INPUT) with anti-Myc (dark blue) and anti-HA (purple) antibodies was carried out to confirm successful protein production. The same samples were used for immunoprecipitation (IP) with anti-Myc followed by immunodetection with anti-Myc (to confirm successful IP) or anti-HA (to identify co-immunoprecipitated partners). Predicted protein molecular weights (KDa): PRK-Myc, 52.1; SlG1-Myc, 56.9; SlG1-HA 47.8.

SUPPORTING TABLES

Table S1. List of primers used in this work

Use	#	Name	Sequence (5'-3')[1]
Cloning	1	SlG1-attB1-F	**GGGGACAAGTTTGTACAAAAAAGCAGGCTGG**ATGGCATTTTTAGCTACCATTTCTG
	2	SlG1-attB2-R	**GGGGACCACTTTGTACAAGAAAGCTGGGTG**ATTCTGTCGATTTGCAATATAACTAGC
	3	SlPSY3-attB1-F	**GGGGACAAGTTTGTACAAAAAAGCAGGCTGG**ATGTGTCCAGCAACACTTTCTTATT
	4	SlPSY3-attB2-R	**GGGGACCACTTTGTACAAGAAAGCTGGGTG**TTGAATGGCTAAACTAGGCAAAGATAAAG
	5	AtPRK-attB1-F	**GGGGACAAGTTTGTACAAAAAAGCAGGCT**ATGGCTGTCTCAACTATCTAC
	6	AtPRK-attB2-R	**GGGGACCACTTTGTACAAGAAAGCTGGGT**CGGCTTTAGCTTCTGCACGAGC
RT-qPCR	7	SlPSY1-qPCR-F	ACAGGCAGGTCTATCCGATG
	8	SlPSY1-qPCR-R	ACGCCTTTCTCTGCCTCATC
	9	SlPSY2-qPCR-F	CAGGGCTCTCCGATGAAGAC
	10	SlPSY2-qPCR-R	CACCGGCCATCTACTAGCAG
	11	SlPSY3-qPCR-F	TTGGATGCAATAGAGGAGAATG
	12	SlPSY3-qPCR-R	ATTGAATGGCTAAACTAGGCAAAG
	13	SlG1-qPCR-F	GGCCTTTGAACATGTGGCTACC
	14	SlG1-qPCR-R	ACTCGCCAAGTCCACAATTTGC
	15	SlG2-qPCR-F	AAAGTCATCGTCGGAGCTCG
	16	SlG2-qPCR-R	GTTTAGCTTCGCCGTTGAGC
	17	SlG3-qPCR-F	AGGAGGTGCACCAGATGAAG
	18	SlG3-qPCR-R	TCAGCAACCAAGTCCTTCCC
	19	SlACT4-qPCR-F	CCTTCCACATGCCATTCTCC
	20	SlACT4-qPCR-R	CCACGCTCGGTCAGGATCT
	21	SlSSUI-qPCR F	GGACAGCTAGAAGGCCAATATC
	22	SlSSUI-qPCR R	GCTCCACATGCATGAATTTCC
sgRNAs for CRISPR-Cas9 gene impairment	23	SlG1-sgRNA-1 F	ATTGGTTCAGCTGTTGGCTCAGAA
	24	SlG1-sgRNA-1 R	AAACTTCTGAGCCAACAGCTGAAC
	25	SlG1-sgRNA-2 F	ATTGGTACATTCACCACCATAAGA
	26	SlG1-sgRNA-2 R	AAACTCTTATGGTGGTGAATGTAC
CRISPR plants genotyping	27	SlG1 Geno F	GCTTGCGCAGTTGAGATGATCC
	28	SlG1 Geno R	GGTCCTTACCCGCTGTCTTTCC
	29	Cas9 F	TCCCTCATCAGATCCACCTC
	30	Cas9 R	CTGAAACGTGAGCCTTCTGG
	31	NTP II F	GAAGGGGATAGAAGGCGA
	32	NTP II R	AGATGGATTGCACGCAGG

[1]Gateway recombination sites in bold

Table S2. Constructs and cloning details.

Use	Construct	Template	Primers[1]	Sequence cloned[2]	Cloning method	Entry plasmid	Destiny plasmid
Co-immunoprecipitation assays	*SlG1-HA*	Tomato root cDNA	1+2	$SlG1_{1-1098}$	Gateway	pDONR207	pGWB414
	SlPSY1-HA	Tomato fruit cDNA		$SlPSY1_{1-1236}$	Gateway	pDONR207	pGWB414
	SlPSY2-HA	Tomato leaf cDNA		$SlPSY2_{1-1314}$	Gateway	pDONR207	pGWB414
	SlPSY3-HA	Tomato root cDNA	3+4	$SlPSY3_{1-1186}$	Gateway	pDONR207	pGWB414
	SlG1-Myc	Tomato root cDNA	1+2	$SlG1_{1-1098}$	Gateway	pDONR207	pGWB420
	SlG2-Myc	Tomato flower cDNA		$SlG2_{1-1089}$	Gateway	pDONR207	pGWB420
	SlG3-Myc	Tomato flower cDNA		$SlG3_{1-1080}$	Gateway	pDONR207	pGWB420
	AtPRK-Myc	Arabidopsis seedling cDNA	5+6	$AtPRK_{1-1556}$	Gateway	pDONR207	pGWB417
CRISPR-Cas9 gene impairment	*pEN-SlG1(sg1)*	-	23+24	$SlG1_{644-664}$	*BbsI* / T4 ligase	pENC1.1	-
	pEN-SlG1(sg2)	-	25+26	$SlG1_{732-752}$	*BbsI* / T4 ligase	pENC1.1	-
	pDE-SlG1(1+2)	*pEN-SlG1(sg1) + (sg2)*	-	$SlG2_{644-664}$ + $SlG2_{732-752}$	(*sg1*)*MluI* + *Bsu36I* / T4 ligase (sg2)Gateway	*pEN-SlG1(sg1) + (sg2)*	pDE-Cas9

[1]Constructs without primers reported in Barja et al.(2021)

[2]Numbers indicate the first and last nucleotide positions cloned from the coding sequence of the indicated gene.

Table S3. Co-expression of tomato GGPPS paralogs (guide genes) with isoprenoid-related genes (query genes) in root tissue. Significant pairwise Pearson correlations between guide and query genes (≥0.55) are highlighted in red (when positive) or green (when negative). Arabidopsis genes were used as queries to search for tomato homologs in PLAZA 4 (https://bioinformatics.psb.ugent.be/plaza/versions/plaza_v4_dicots/). Genes are organized by pathways.

			GGPPS1	GGPPS2	GGPPS3
Pathway/Family	Name	SOL Tomato gene	Solyc11g011240	Solyc04g079960	Solyc02g085700
MEP	DXS1	Solyc01g067890	0,227817285	-0,432217062	0,28528147
MEP	DXS2	Solyc11g010850	0,997036917	-0,103686573	0,326655343
MEP	DXS3a	Solyc01g028900	0,055742093	-0,087928801	0,718940454
MEP	DXS3b	Solyc08g066950	0,639972045	-0,070017463	0,741305712
MEP	DXR1	Solyc03g114340	0,983938259	-0,082546381	0,410076944
MEP	DXR2	Solyc06g060860	0,199524053	0,166352456	-0,292225453
MEP	CMK	Solyc01g009010	0,884968181	0,014512289	0,480860925
MEP	MCT	Solyc01g102820	0,488415714	0,40006911	0,364206591
MEP	MDS	Solyc08g081570	0,213003447	0,122519655	0,623933883
MEP	HDS	Solyc11g069380	0,882686457	0,057137735	0,423279789
MEP	HDR	Solyc01g109300	-0,092325695	-0,444207896	-0,15767962
IDI	IDI1	Solyc08g075390	-0,053766114	-0,27002078	0,408431113
IDI	IDI2	Solyc05g055760	-0,01368272	0,152778807	0,657783139
IDI	IDI3	Solyc04g056390	0,29426506	-0,292380737	0,371964203
GGDR	GGDR1	Solyc01g088310	-0,130952114	0,708765564	-0,384847304
GGDR	GGDR2	Solyc03g115980	-0,396270784	0,152964101	-0,09490842
Tocopherols	HPPD1/PDS1a	Solyc05g041200	-0,003258982	-0,363823003	0,48259298
Tocopherols	HPPD2/PDS1b	Solyc07g045050	0,002860197	-0,071459139	-0,200460026
Tocopherols	VTE2	Solyc07g017770	0,553561893	0,064150277	0,381503736
Tocopherols	VTE3a	Solyc03g005230	0,424721351	0,110779221	0,105863188
Tocopherols	VTE3b	Solyc09g065730	0,228218686	0,081748204	0,610840864
Tocopherols	VTE1	Solyc08g068570	0,616813434	0,325744429	0,431115249
Tocopherols	VTE4a	Solyc08g076360	-0,151515162	0,236492581	0,506975932
Tocopherols	VTE4b	Solyc04g063230	-0,110780823	0,36361524	-0,302450315
Tocopherols	VTE4c	Solyc08g077240	-0,303071631	-0,145364926	-0,583830612
Tocopherols	VTE4d	Solyc03g116150	-0,290047454	-0,003146301	0,334972422
Chlorophyll synthesis	HEMA1	Solyc04g076870	-0,105259917	-0,274261136	0,419202338
Chlorophyll synthesis	HEMA2	Solyc01g106390	0,040718913	-0,159382416	0,72009636
Chlorophyll synthesis	HEMA3	Solyc01g089840	#N/D	#N/D	#N/D
Chlorophyll synthesis	GSA	Solyc04g009200	-0,082894254	-0,089319358	0,612747431
Chlorophyll synthesis	HEMB	Solyc08g069030	-0,151430238	-0,405537832	0,478103613
Chlorophyll synthesis	HEMC	Solyc07g066470	-0,071151521	0,459018759	0,129818671
Chlorophyll synthesis	HEMD	Solyc04g079320	0,469479524	-0,246514255	0,214036299
Chlorophyll synthesis	HEME1	Solyc10g007320	0,465700714	0,057792204	0,15566927
Chlorophyll synthesis	HEME2	Solyc06g048730	0,211799103	-0,094178477	0,065673668
Chlorophyll synthesis	HEMF	Solyc10g005110	0,665308945	0,044622375	0,339341703
Chlorophyll synthesis	HEMG1	Solyc01g079090	0,117133036	-0,407554853	0,350194089
Chlorophyll synthesis	HEMG2	Solyc03g005080	0,467537798	-0,369333515	0,659054874
Chlorophyll synthesis	CHLH	Solyc04g015750	-0,26701238	-0,110482093	-0,566896786
Chlorophyll synthesis	CHLI	Solyc10g008740	0,594459595	-0,038296053	-0,114544313
Chlorophyll synthesis	CHLD	Solyc04g015490	0,556081009	-0,167039536	0,183230703
Chlorophyll synthesis	CHLM	Solyc03g118240	0,458485616	0,400565799	0,182033019
Chlorophyll synthesis	CHL27-CRD	Solyc10g077040	-0,223630138	-0,00816874	-0,307798293
Chlorophyll synthesis	DVR	Solyc01g067290	-0,010768598	0,348905198	0,097673629
Chlorophyll synthesis	PORA	Solyc12g013710	-0,134290208	-0,112528933	0,241062199
Chlorophyll synthesis	PORB	Solyc07g054210	-0,196642498	-0,364421753	-0,136536604
Chlorophyll synthesis	PORC	Solyc10g006900	0,099037913	0,045790641	-0,121562843
Chlorophyll synthesis	CHLG1	Solyc05g024190	-0,162371852	0,001311095	0,31995561
Chlorophyll synthesis	CHLG2	Solyc09g014760	0,467429605	0,065746944	-0,1716427
Chlorophyll synthesis	CAOa	Solyc06g060310	-0,140415216	-0,307867459	-0,346880611
Chlorophyll synthesis	CAOb	Solyc11g012850	-0,134284865	-0,135540982	0,160700206

			GGPPS1	GGPPS2	GGPPS3
Pathway/Family	Name	SOL Tomato gene	Solyc11g011240	Solyc04g079960	Solyc02g085700
Chlorophyll degradation	CHL1	Solyc09g065620	#N/D	#N/D	#N/D
Chlorophyll degradation	CHL2a	Solyc06g053980	0,135263552	0,414254359	-0,090432445
Chlorophyll degradation	CHL2b	Solyc09g082600	-0,189527461	-0,431145721	-0,485581871
Chlorophyll degradation	CHL2c	Solyc12g005300	0,063207593	0,494543447	-0,189462652
Chlorophyll degradation	CLD1	Solyc02g070490	0,097418732	-0,019030447	-0,121496138
Chlorophyll degradation	SGR1	Solyc08g080090	0,334525535	0,351924964	0,239984752
Chlorophyll degradation	SGR2	Solyc12g056480	#N/D	#N/D	#N/D
Chlorophyll degradation	SGR3	Solyc04g063240	#N/D	#N/D	#N/D
Chlorophyll degradation	PPH	Solyc01g088090	-0,02570926	0,102250436	0,624178482
Chlorophyll degradation	PAO1	Solyc11g066440	0,075470096	-0,407248086	0,574465029
Chlorophyll degradation	PAO2	Solyc04g040160	#N/D	#N/D	#N/D
Chlorophyll degradation	PAO3	Solyc12g096550	-0,441818414	-0,426715473	-0,264975363
Chlorophyll degradation	RCCR	Solyc03g044470	0,252496332	-0,050336257	0,221137805
Chlorophyll degradation	PK1	Solyc03g071720	0,306310405	-0,274536284	0,638200534
Chlorophyll degradation	PK2	Solyc09g018510	-0,002769879	-0,124326081	-0,192384004
Chlorophyll degradation	NYC1	Solyc07g024000	0,079814353	-0,037916608	0,65448831
Chlorophyll degradation	CBR/NOL	Solyc05g032660	0,747124715	0,111886245	0,146036329
Chlorophyll degradation	HCAR	Solyc09g091100	-0,0128925	-0,289975445	-0,294073066
Phyllooquinone	ICS1/MENF	Solyc06g071030	#N/D	#N/D	#N/D
Phyllooquinone	PHYLLO/MEND1	Solyc04g005190	0,610474528	-0,184506979	0,118924512
Phyllooquinone	PHYLLO/MEND2	Solyc04g005200	0,622287417	0,021210242	-0,02088809
Phyllooquinone	PHYLLO/MEND3	Solyc04g005180	0,475484562	-0,108459214	0,163378551
Phyllooquinone	AAE14	Solyc02g069920	0,06366328	0,073537116	-0,109614114
Phyllooquinone	DHNS/MENB	Solyc05g005180	0,811508543	-0,001651354	0,216802597
Phyllooquinone	DHNAT1	Solyc02g078410	-0,143053242	-0,125034472	0,501479632
Phyllooquinone	DHNAT2	Solyc03g006440	#N/D	#N/D	#N/D
Phyllooquinone	DHNAT3	Solyc03g006450	#N/D	#N/D	#N/D
Phyllooquinone	ABC4	Solyc01g105460	0,45668733	0,076177322	0,606850632
Phyllooquinone	MENG	Solyc12g019010	0,355667655	-0,429933867	-0,182348
Plastoquinone	TAT7/HPPS1	Solyc10g007110	-0,211383766	0,21345445	-0,302773187
Plastoquinone	TAT7/HPPS2	Solyc12g088000	-0,23856167	0,12907316	-0,477127228
Plastoquinone	TAT7/HPPS3	Solyc12g096240	-0,183757802	0,101931181	0,050024062
Plastoquinone	PDS2/HST	Solyc03g051810	0,449387501	-0,187413559	0,21955408
Plastoquinone	AAAT1	Solyc07g053720	-0,015951791	-0,366235433	0,43220791
Plastoquinone	AAAT2	Solyc10g008200	0,217492085	0,566893925	0,166994149
Plastoquinone	AAAT3	Solyc07g053710	0,17507915	0,196294288	0,588052247
Plastoquinone	ACS12	Solyc03g007070	-0,050853036	-0,291718623	-0,376091867
Plastoquinone	TAA1	Solyc05g031600	-0,259243414	-0,139275642	-0,375694205
Carotenoids	PSY1	Solyc03g031860	0,48436295	-0,068458482	0,183689089
Carotenoids	PSY2	Solyc02g081330	-0,372992877	0,255376259	-0,563151392
Carotenoids	PSY3	Solyc01g005940	0,9887403	-0,031173898	0,291125507
Carotenoids	PDS	Solyc03g123760	0,993379539	-0,045712605	0,322656275
Carotenoids	ZDS	Solyc01g097810	0,960459119	-0,021713467	0,302818591
Carotenoids	Z-ISO	Solyc12g098710	0,738619978	-0,091519099	0,551931703
Carotenoids	CRTISO1	Solyc10g081650	0,943765101	-0,100731764	0,464601885
Carotenoids	CRTISO2	Solyc05g010180	#N/D	#N/D	#N/D
Carotenoids	LCY-B1	Solyc04g040190	-0,060826955	0,034921071	0,126715816
Carotenoids	LCY-B2 (CYC-B)	Solyc10g079480	0,47083548	0,004718384	0,258287127
Carotenoids	LCY-E	Solyc12g008980	#N/D	#N/D	#N/D
Carotenoids	BCH1	Solyc06g036260	-0,494401783	-0,110140751	-0,278124838
Carotenoids	BCH2	Solyc03g007960	0,022206108	0,123623457	-0,182607406
Carotenoids	CYP97B3	Solyc05g016330	0,247342197	-0,15114203	-0,143317243
Carotenoids	CYP97A3	Solyc04g051190	0,934087572	0,079186798	0,433488572
Carotenoids	CYP97C1	Solyc10g083790	0,656435414	0,092000116	0,720760803
Carotenoids	ZEP1	Solyc06g060880	0,092497037	0,119284103	-0,356821625
Carotenoids	NSY1	Solyc02g089050	-0,141068334	0,150647962	-0,429764058
Carotenoids	VDE	Solyc04g050930	0,710345593	0,09745212	0,163692149

			GGPPS1	GGPPS2	GGPPS3
Pathway/Family	Name	SOL Tomato gene	Solyc11g011240	Solyc04g079960	Solyc02g085700
Carotenoid degradation	CCD1A	Solyc01g087250	0,897385096	-0,097410517	0,413828304
Carotenoid degradation	CCD1B	Solyc01g087260	-0,486507306	-0,319343808	0,12600825
Carotenoid degradation	CCDX	Solyc08g066720	0,962831828	0,005214157	0,244918912
Carotenoid degradation	CCD4A	Solyc08g075480	#N/D	#N/D	#N/D
Carotenoid degradation	CCD4B	Solyc08g075490	#N/D	#N/D	#N/D
Orange	Or1	Solyc03g093830	0,956695311	-0,047672533	0,407062323
Orange	Or2	Solyc09g010110	0,429020461	-0,375775452	0,375550783
ABA	NCED2	Solyc08g016720	0,877409595	0,007780788	0,427354139
ABA	NCED3	Solyc07g056570	0,471895819	0,112222671	0,570947911
ABA	NCED6	Solyc05g053530	#N/D	#N/D	#N/D
ABA	ABA2a	Solyc04g071940	0,028984238	0,338164225	-0,549218342
ABA	ABA2b	Solyc04g071960	#N/D	#N/D	#N/D
ABA	ABA2c	Solyc10g085380	-0,288588412	0,346337388	-0,511417212
ABA	ABA2d	Solyc11g018600	#N/D	#N/D	#N/D
ABA	AAO3a	Solyc11g065920	0,053296522	-0,464463544	0,571416643
ABA	AAO3b	Solyc11g065930	-0,22308611	0,03808593	0,499516268
ABA	ABA3	Solyc07g066480	0,498915173	0,063687929	0,200693733
ABA	ABA4	Solyc02g063170	-0,388641886	-0,152190581	-0,427829713
ABA	CYP707A1	Solyc04g078900	#N/D	#N/D	#N/D
ABA	CYP707A2	Solyc08g075320	0,121000641	-0,263589633	-0,418754624
ABA	CYP707A3a	Solyc01g108210	0,191959425	-0,166036381	0,502077133
ABA	CYP707A3b	Solyc08g005610	0,005129081	-0,321170606	-0,244657287
ABA	CYP707A3c	Solyc04g071150	0,911640177	-0,093816362	0,087467239
ABA	CYP707A3d	Solyc04g080650	-0,279642404	0,32164075	0,116087837
ABA	ABA1/ZEP	Solyc02g090890	-0,51934943	-0,030013217	-0,538058819
ABA	NSY3	Solyc02g086050	0,185788857	0,303292174	0,269656709
ABA	NSY5	Solyc06g074240	0,992272356	-0,075441014	0,340861095
SLs	MAX3 (CCD7)	Solyc01g090660	0,992904154	-0,106902828	0,300371981
SLs	MAX1	Solyc08g062950	0,986086882	-0,065425469	0,276445814
SLs	MAX4 (CCD8)	Solyc08g066650	0,996596827	-0,059714661	0,297058985
Giberellins	CPS1	Solyc06g084240	0,997400089	-0,102023381	0,306665528
Giberellins	CPS2	Solyc08g005710	#N/D	#N/D	#N/D
Giberellins	CPS3	Solyc09g065230	#N/D	#N/D	#N/D
Giberellins	KS1a	Solyc07g066670	0,797763542	0,116676707	0,341005665
Giberellins	KS1b	Solyc08g005720	0,45802595	0,427222273	-0,164064737
Giberellins	GA3	Solyc04g083160	0,99177426	-0,02644603	0,273361971
Giberellins	KAO1	Solyc01g080900	0,925218611	0,063463248	0,195364444
Giberellins	KAO2	Solyc08g007050	#N/D	#N/D	#N/D
Giberellins	KAO3	Solyc12g006460	-0,043884958	0,538148128	0,135522157
Giberellins	KAO4	Solyc10g007860	#N/D	#N/D	#N/D
Giberellins	GA20ox1	Solyc03g006880	0,990700671	-0,061266037	0,279604246
Giberellins	GA20ox2	Solyc09g009110	#N/D	#N/D	#N/D
Giberellins	GA20ox3	Solyc11g072310	0,764067607	0,079907645	0,030099693
Giberellins	GA20ox4	Solyc06g035530	#N/D	#N/D	#N/D
Giberellins	GA20ox5	Solyc01g093980	0,979136723	-0,070374827	0,274557014
Giberellins	GA20ox6	Solyc06g050110	#N/D	#N/D	#N/D
Giberellins	GA20ox7	Solyc11g013360	#N/D	#N/D	#N/D
Giberellins	GA3ox1	Solyc06g066820	0,97438317	-0,042467304	0,262767095
Giberellins	GA3ox2	Solyc03g119910	#N/D	#N/D	#N/D
Giberellins	GA3ox3	Solyc00g007180	#N/D	#N/D	#N/D
Giberellins	GA3ox4	Solyc01g058250	-0,158328167	-0,133515069	0,596201491
Giberellins	GA3ox5	Solyc05g052740	#N/D	#N/D	#N/D

754

			GGPPS1	GGPPS2	GGPPS3
Pathway/Family	**Name**	**SOL Tomato gene**	**Solyc11g011240**	**Solyc04g079960**	**Solyc02g085700**
MVA pathway	HMGS1	Solyc08g080160	#N/D	#N/D	#N/D
MVA pathway	HMGS2	Solyc08g007790	-0,082203011	-0,171648603	0,636394447
MVA pathway	HMGS3	Solyc12g056450	0,108375307	-0,083799696	-0,282527204
MVA pathway	HMGS4	Solyc08g080170	-0,119184485	0,064018582	0,67219755
MVA pathway	HMGR1	Solyc03g032020	0,233838251	-0,269895899	0,493862077
MVA pathway	HMGR2	Solyc02g082260	-0,243850449	-0,482597207	-0,321043725
MVA pathway	HMGR3	Solyc02g038740	-0,08065974	-0,159039759	0,64130647
MVA pathway	HMGR4	Solyc03g032010	0,448026273	0,140362687	0,252487654
MVA pathway	MVK	Solyc01g098840	-0,101188848	-0,192849616	0,63006538
MVA pathway	PMK1	Solyc08g076140	0,118637298	-0,392787149	0,587969204
MVA pathway	PMK2	Solyc06g066310	0,063436412	-0,060619985	0,729922806
MVA pathway	MVD1	Solyc04g009650	0,028841528	0,197760815	0,612150651
MVA pathway	MVD2	Solyc11g007020	-0,120558081	-0,097527905	0,629381981
MVA pathway	AACT1	Solyc05g017760	0,185899173	0,615360485	0,347271304
MVA pathway	AACT2	Solyc07g045350	-0,108831687	-0,122710038	0,650776949
MVA pathway	AACT3	Solyc04g015100	0,088470241	0,04828122	0,728496447
FDS	FDS1	Solyc10g005840	0,523849783	-0,102281461	0,102421253
FDS	FDS2	Solyc12g015860	-0,079504135	-0,031898035	0,637541783
FDS	FDS3	Solyc10g005810	0,4018755	0,248462877	0,32880738
FDS	FDS4	Solyc10g005820	0,375810018	0,419812374	0,253962811
Ubiquinone	PPT1	Solyc03g114300	0,388805365	-0,095730347	0,673083897
Ubiquinone	CoQ3	Solyc07g055850	0,43200067	0,35963032	0,07331323
Ubiquinone	CoQ5a	Solyc01g081470	0,074871819	0,06013107	0,559041736
Ubiquinone	CoQ6	Solyc09g091570	0,68029036	-0,227989585	0,196851133